



OPEN

Environmental influences on sinking rates and distributions of transparent exopolymer particles after a typhoon surge at the Western Pacific

M. Shahanul Islam^{1,3}, Jun Sun^{2,3}✉, Guicheng Zhang³, Zhuo Chen³ & Hui Zhou⁴

A multidisciplinary approach was used to investigate the causes of the distributions and sinking rates of transparent exopolymer particles (TEPs) during the period of September–October (2017) in the Western Pacific Ocean (WPO); the study period was closely dated to a northwest typhoon surge. The present study discussed the impact of biogeophysical features on TEPs and their sinking rates (sSTEP) at depths of 0–150 m. During the study, the concentration of TEPs was found to be higher in areas adjacent to the Kuroshio current and in the bottom water layer of the Mindanao upwelling zone due to the widespread distribution of cyanobacteria, i.e., *Trichodesmium hildebrandti* and *T. theibauti*. The positive significant regressions of TEP concentrations with Chl-a contents in eddy-driven areas ($R^2 = 0.73$, especially at 100 m ($R^2 = 0.75$)) support this hypothesis. However, low TEP concentrations and TEPs were observed at mixed layer depths (MLDs) in the upwelling zone (Mindanao). Conversely, high TEP concentrations and high sSTEP were found at the bottom of the downwelling zone (Halmahera). The geophysical directions of eddies may have caused these conditions. In demonstrating these relations, the average interpretation showed the negative linearity of TEP concentrations with TEPs ($R^2 = 0.41 \sim 0.65$) at such eddies. Additionally, regression curves ($R^2 = 0.78$) indicated that atmospheric pressure played a key role in the changes in TEPs throughout the study area. Diatoms and cyanobacteria also curved the TEPs significantly ($R^2 = 0.5$, $P < 0.05$) at the surface of the WPO. This study also revealed that TEP concentration contributes less to the average particulate organic carbon in this oligotrophic WPO.

Generally, polysaccharide-based transparent exopolymer particles (TEPs) are derived from microorganisms, i.e., phytoplankton^{1–5}, depending on their physiological state^{6,7} and bloom condition^{4,8}. This secretion is also influenced by various environmental conditions, i.e., chlorophyll-*a* (chl-*a*)⁹, nutrient content¹⁰, salinity¹¹, turbulence^{12,13} and CO₂ concentration in the water¹⁴. However, the production of TEPs associated with phytoplankton mainly depends on the concentrations of diatoms^{15,16} and cyanobacteria¹⁷. As an oil droplet¹, TEP secretion is a defense mechanism of phytoplankton; these secretions aggregate at the surface³ of the ocean and contribute to atmospheric carbon by bubble bursting or wave action⁴. In addition, TEPs occasionally act as food sources for zooplankton across the ocean^{17,18}.

Complex correspondences of TEPs with phytoplankton and environmental conditions were reviewed in previous studies¹⁹. They reported that the relation between phytoplankton compositions and oceanographic processes is complex through the western boundary currents²⁰. For example, phytoplankton blooms have been reported on currents that drive upwelling²¹, which may amplify TEPs along adjacent areas^{4,8}. However, TEPs have been reported to be higher in coastal areas^{22,23}, especially in estuaries^{24,25}, rather than in the open ocean^{26–29}. More

¹College of Food Engineering and Biotechnology, Tianjin University of Science and Technology University, TEDA, No 29, 13th Avenue, Tianjin, China. ²College of Marine Science and Technology, China University of Geosciences (Wuhan), Wuhan 430074, China. ³Research Centre for Indian Ocean Ecosystem, Tianjin University of Science and Technology, Tianjin 300457, China. ⁴Key Laboratory of Ocean Circulation and Waves, and Institute of Oceanology, Chinese Academy of Sciences, Qingdao Collaborative Innovation Center of Marine Science and Technology, Qingdao 266071, China. ✉email: phytoplankton@163.com

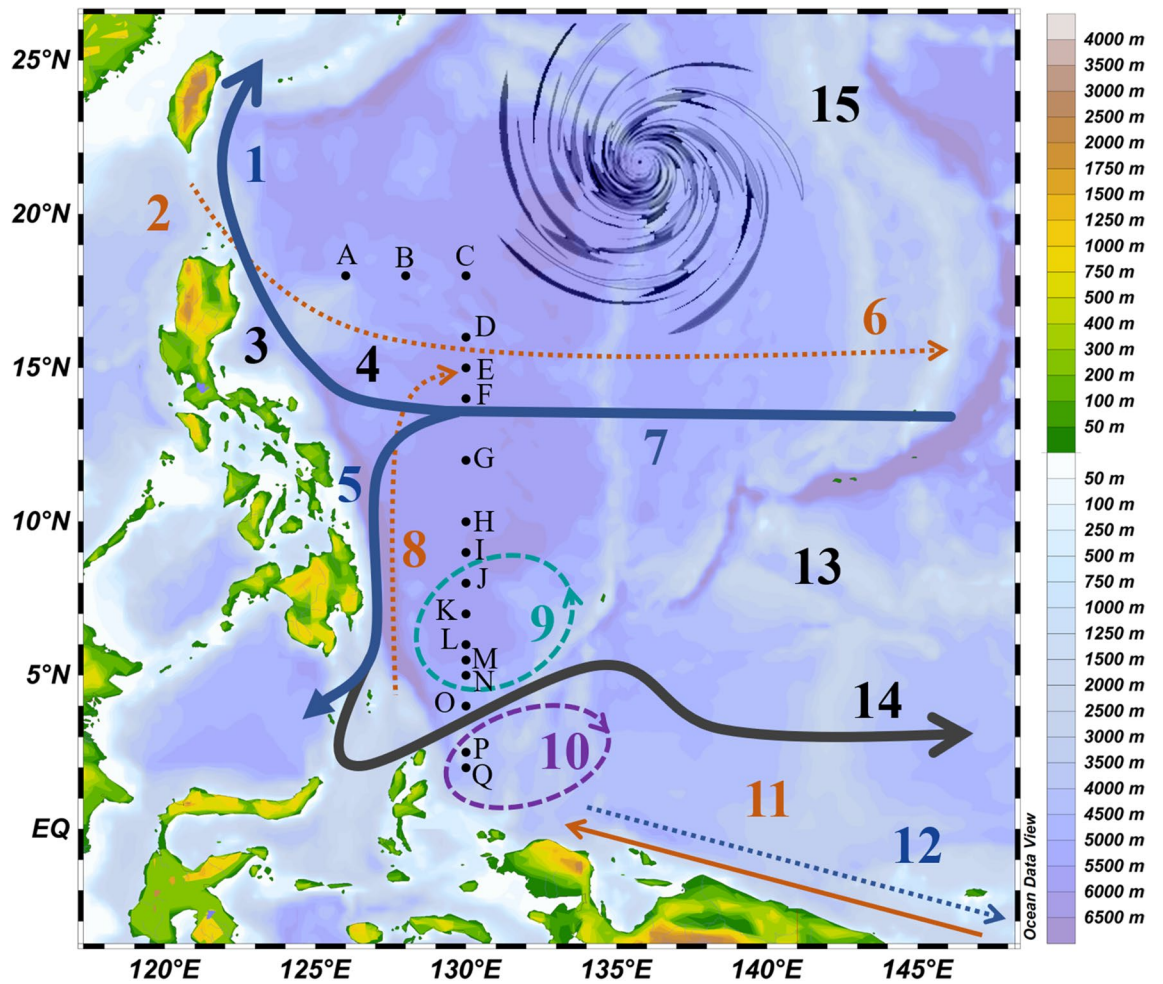


Figure 1. Sampling stations (St. A–Q) with different local currents (A), i.e., 7 = North Equatorial current (NEC), 6 = North Equatorial under current (NEUC), 14 = North Equatorial counter current (NECC), 1 = Kuroshio current (KC), 2 = Luzon Under current (LUC), 5 = Mindanao current (MC), 8 = Mindanao under current (MUC), 11 = New Guinea coastal current (NGCC), and 12 = New Guinea coastal under current (NGCUC), with the related geo-physical forcings, i.e., 9 = Mindanao Eddy (ME), 10 = Halmahera Eddy (HE), 3 = Philippine trenches (PT) in the Western Pacific Ocean (WPO). Additionally, Typhoon Lan⁴⁵ occurred near the Philippine coast during the sampling period in the WPO (13).

specifically, high TEPs have been found at mixed layer depths (MLDs) in the ocean due to their ability to stick to each other^{4,30}. It was also reported that the TEP concentrations²⁸ and sinking rate (sTEP)²⁴ were higher in the surface current active zone of marine environments. Beside current activities, Low sTEP may affect by TEPs for its stickiness^{8,19}. Therefore, local geophysical features may influence the concentration and sinking rates of TEPs through external forcing. Likewise, TEPs are also hypothesized to be affected indirectly or actively by eddies and oceanic circulations. Considering these phenomena, the Western Pacific Ocean (WPO) is a suitable study area, as it hosts numerous circulations and eddies³¹.

Open ocean currents, particularly the boundary currents of the WPO, are referred to as unproductive zones compared to the Eastern Pacific Ocean (EPO) boundary currents²⁰ and coastal areas^{32–35}, as they displace the upper layer of productive waters, mostly in polar regions^{20,36,37}. The WPO water column (Fig. 1) is influenced by various currents³¹, i.e., the North Equatorial current (NEC), North Equatorial undercurrent (NEUC), North Equatorial counter current (NECC), Kuroshio current (KC), Luzon undercurrent (LUC), Mindanao current (MC), Mindanao undercurrent (MUC), New Guinea coastal current (NGCC), and New Guinea coastal undercurrent (NGCUC); vortices^{38,39}, i.e., the Mindanao Eddy (ME) and Halmahera Eddy (HE); and local geological features, i.e., the Philippine trench (PT), Philippine Basin (PB), and Kyushu Palau Ridge (KPR), which influence species biodiversity, nutrient distribution and particles transportation^{40,41}.

Previously, western boundary currents have been reported as intensive circulations of nutrients that may directly affect the local phytoplankton community⁴² and occurrence of particle sinking^{20,24,37}. However, the effect of ocean water circulations (currents, eddies, etc.) on TEPs has remained unclear. The present study was designed to determine the effects of biological parameters influenced by ocean circulations on the distribution of TEPs⁴³ and sTEP, as well as the associated carbon concentrations (TEP_C), at different depths of the WPO⁴⁴. The present study was conducted 4 days after the attack of super typhoon (category 4) Lan⁴⁵, which may have

also locally affected the TEP distribution (Fig. 1). To uncover its causes and effects, correlations between TEPs and sTEP with other environmental parameters will be investigated after considering WPO eddies and current patterns accordingly.

Results

Western pacific hydrology. The vertical zonation of the Western Pacific water column and its features are important to understanding current findings. Previously, WPO water masses were categorized into different sections⁴⁶, i.e., North Pacific tropical water (NPTW) near 11° N^{47,48}, North Pacific intermediate water (NPIW) near 7° N^{49,50}, North Pacific tropical subsurface water (TSSW) between the NPTW and SPTW⁵¹, South Pacific tropical water (SPTW) and Antarctic intermediate water (AAIW) near 1° N^{52–56}, with an intertropical convergence zone (ITCZ) between 4°–8° N⁵⁷. Most of the study stations were aligned on the gridline of 130° E (Fig. 1), covering a depth of 0–150 m, which included the subsurface chlorophyll maximum (SCM) layer. Therefore, this transect was divided into three vertical water layers²⁷, i.e., the MLD (0–50 m), SCM (50–100 m) and depths below the SCM (BSCM; 100–150 m) rather than two layers, as reported in previous studies⁵⁸. These segmentations were also supported by T-S clustering of the sampling stations into three groups (Fig. 2A), which may further explain the vertical congregations of TEPs (Fig. 2B).

Geo-physical zonation of stations. Station zonation and associations were relatively dependent on the geophysical positions and directions of currents and eddies⁵⁹. The width of the NEC was reported to be between 8 and 18° N, and that of the NECC was between 2 and 7° N⁶⁰. Kuroshio started after 127° E from NEC bifurcation³¹. Therefore, stations A and B in the present study were associated with the KC (S_{KC}) and C-I of the NEC (S_{NEC}). Generally, 126.7–128° E is considered the width of the MC, and its undercurrent (MUC) was detected from 400 m below the MC³¹. Additionally, the NEUC existed 200 m below the NEC⁶⁰. Therefore, the sampling area (130°E) is far from the MC, and the sampling depths (0–150 m) were not influenced by undercurrents in the WPO (MUC and NEUC). According to the literatures^{31,59,61–63} and real-time surface geostrophic velocity data, it was found that stations J–N were associated with the ME (denoted as S_{ME}), and P and Q were associated with the HE (S_{HE}). This is also supported by stations' cluster analysis (Pearson coefficient) after considering nutrients as variables (Fig. 2C). Furthermore, the position of Station (St.) O (at eddy edge area) was temporarily affected by the NECC (Fig. 1). Despite having an average marginal position between Mindanao and Halmahera (Fig. 1), St. O falls under S_{HE} due to its high TEP_s, such as that at P and Q (1.7 mD⁻¹). They all constitute a substantial contribution to explaining TEP concentrations in the WPO (Fig. 2D). The study transect possessed high temperatures (> 30 °C) with comparatively low salinity levels (< 34.5 psu) at the surface compared to its bottom. However, salinity was relatively high at the MLD of St. C along compared to the NEC than other stations with low temperature. Temperature (Fig. 3A) and salinity (Fig. 3B) were randomly stratified at stations J to N through the upwelling zone of the cold Mindanao eddy (Fig. 1).

Nutrients and Plankton composition. The average phytoplankton communities were composed of 70% diatoms, where 16% were cyanobacteria and 14% were dinoflagellates. The dominant diatoms were *Nitzschia* sp., *Cerataulus smithii*, *Proboscia alata*, *Nitzschia palea*, and *Nitzschia filiformis*. Dinoflagellates, i.e., *Pyrophacus horologium*, *Gyrodinium spirale*, *Prorocentrum lenticulatum*, and cyanobacteria, i.e., *Trichodesmium hildebrandti* and *T. theibauti*, were also common in the WPO. Analysis showed that the average Chl-*a* was high in the SCM layer of stations M–Q (Fig. 3C). However, a higher chl-*a* content was found below the SCM of stations C–G (Fig. 3C) due to the higher abundance of dinoflagellates (Fig. 4B). However, greater abundances of Chl-*a* P (Fig. 3D) and chl-*a* N (Fig. 3E) were observed at the SCM of stations O, P and Q due to the activity of warm HEs (Fig. 1), with high chl-*a* M at the MLD (Fig. 3F). The high abundance of phytoplankton (Fig. 4C), especially diatoms (Fig. 3D) and cyanobacteria (Fig. 3E), may be liable for these scenarios. In addition, the abundance of zooplankton was found to be higher at the surface of S_{ME} and at the BSCM of S_{NEC} (Fig. 4F), which may also indicate phytoplankton availability in these zones.

The contents of all nutrients (except NO₄) were higher at stations G to J (Fig. 3) at the MLD. Stations O, P and Q possessed dense NO₂ concentrations throughout their whole area (Fig. 3K), especially at the subsurface area. Ammonia (NH₄) was found to be higher at the surface of stations B, C and D (Fig. 3L). The highest concentrations of nutrients (PO₄, NO_x, NO₃ and SiO₃) were found below the SCM at stations I to Q (Fig. 3).

TEP concentration and distribution. The concentration of TEPs was found to be $6.59 \pm 7.52 \mu\text{g Xeq L}^{-1}$ on average throughout the WPO. The highest average concentration was $20.72 \mu\text{g Xeq L}^{-1}$ at St. I and lowest average concentration was $2.29 \mu\text{g Xeq L}^{-1}$ at St. D. It was also found to be higher at 150 m depth at stations I, J, M and N (Fig. 4G). The average horizontal TEP distribution was higher (Fig. 5A) within the S_{ME} area ($7.37 \pm 7.5 \mu\text{g Xeq L}^{-1}$) and lower across the S_{HE} ($5.76 \pm 2.3 \mu\text{g Xeq L}^{-1}$) than in other areas (Table 1). Vertically, the TEP concentration was higher at the BSCM of S_{ME} ($12.29 \pm 14.91 \mu\text{g Xeq L}^{-1}$) and at the MLD of the S_{KC} ($7.13 \pm 5.21 \mu\text{g Xeq L}^{-1}$). Average calculations also supported these patterns (Fig. 2D). The highest TEP concentration was found at 150 m at St. I in the NEC ($51.80 \mu\text{g Xeq L}^{-1}$), and the lowest concentration was $0.69 \mu\text{g Xeq L}^{-1}$ at 150 m in St. O. At the SCM, S_{HE} possessed a higher TEP concentration ($6.32 \pm 2.45 \mu\text{g Xeq L}^{-1}$) and a lower concentration at the bottom (BSCM) layer ($4.36 \pm 5.45 \mu\text{g Xeq L}^{-1}$) than the other stations (Table 1). S_{NEC} continued to have the lowest TEP concentrations at the MLD ($5.27 \pm 4.66 \mu\text{g Xeq L}^{-1}$) and SCM ($4.98 \pm 3.71 \mu\text{g Xeq L}^{-1}$) during the sampling periods.

Furthermore, TEP_C showed a stratification gradient similar to that of TEP due to its association and relation with TEP_{color} (Fig. 4H). Horizontally, the zonal average TEP_C was $4.94 \pm 5.64 \mu\text{g C L}^{-1}$ (1.71–15.53 $\mu\text{g C L}^{-1}$), with the lowest concentration at St. O ($0.51 \mu\text{g C L}^{-1}$) and highest at the BSCM of St. I ($38.85 \mu\text{g C L}^{-1}$). The SCM

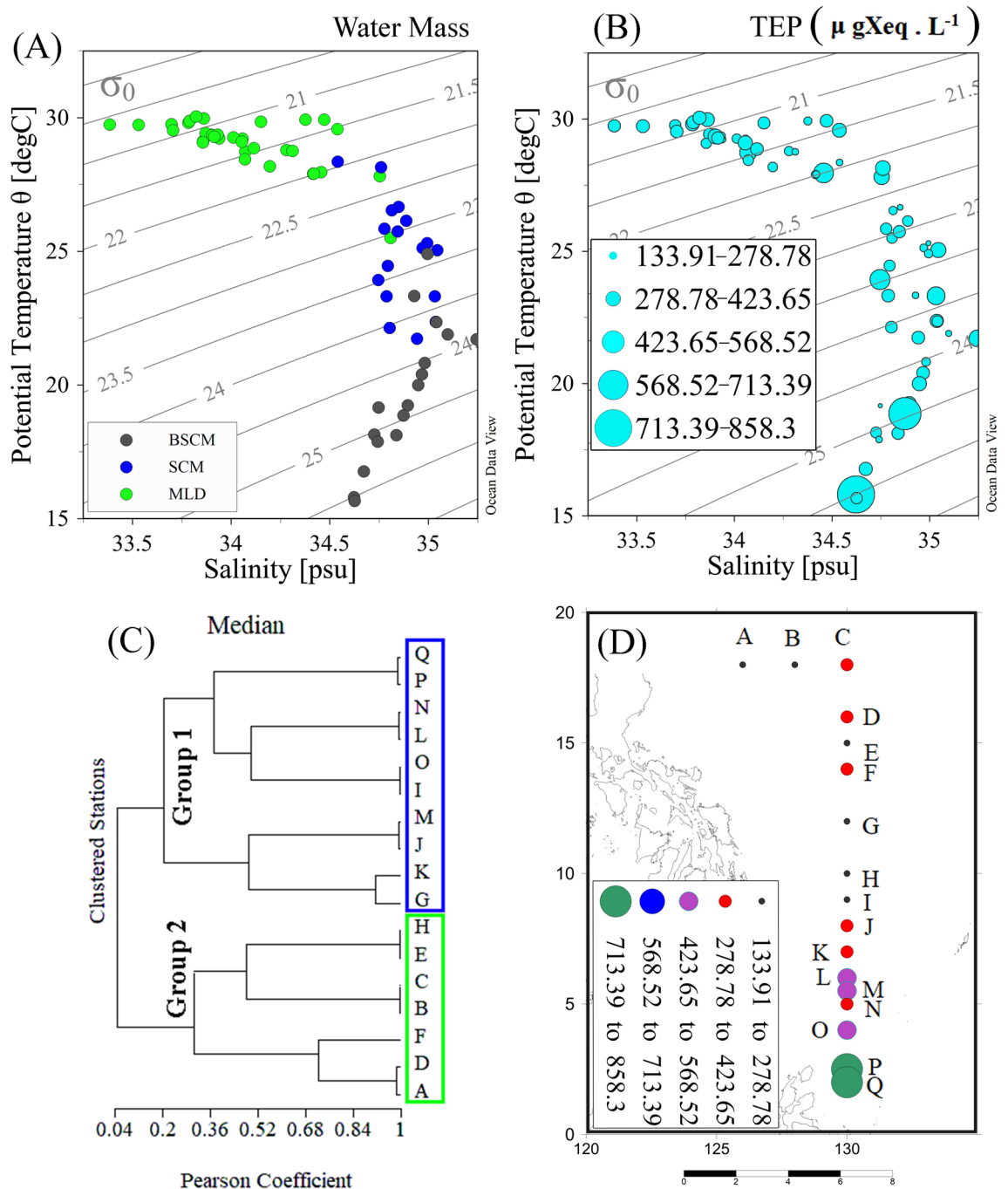


Figure 2. TS diagram of samples with water density gradients (A) compared to TEP concentrations along those water masses (B). Cluster analysis of all stations considering nutrients as variables (C) and average TEP concentrations (D) at the WPO.

layer, especially that at a depth of 50 m, possessed lowest average TEP_C (3.83 $\mu\text{g C L}^{-1}$) compared to other vertical layers (0 m, 100 m and 150 m). The ranges or distribution patterns of TEP_C varied greatly at a depth of 100 m. Moderate variability of the TEP_C distribution was found at 0 m with a higher median (Fig. 5B). Variations in TEP_C abundances were found at S_{NEC} (Fig. 5C).

TEP sinking rates throughout the WPO. The sinking rates of TEPs (sTEP) were determined using the SETCOL method on the deck of the research vessel. The average sTEP was $1.28 \pm 0.37 \text{ mD}^{-1}$, and the highest sedimentation rate was at 150 m at station P ($2.28 \pm 1.5 \text{ mD}^{-1}$) in Halmahera due to the combined effects of the NECC (Fig. 1) and the clockwise anticyclonic rotation of HES^{10,62}. However, the lowest sinking rate was found at 150 m at St. I (0.39 mD^{-1}) as a result of the ME (Fig. 6A) due to the anticlockwise cyclonic upwelling associated with Mindanao. Depthwise (0, 50, 100 and 150 m) average sinking rates were higher at 100 m ($1.32 \pm 0.98 \text{ mD}^{-1}$),

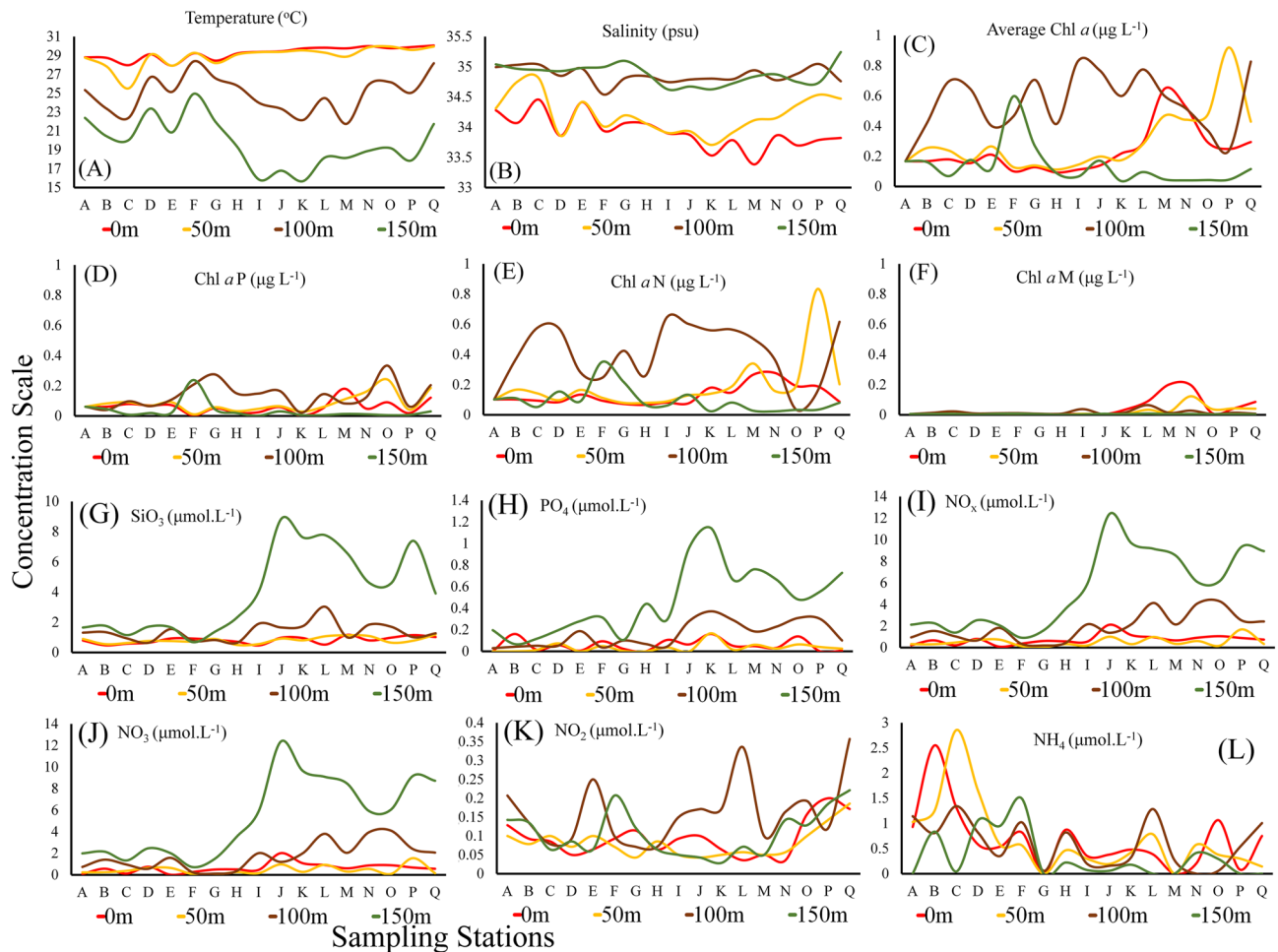


Figure 3. Different environmental parameters, i.e., Temperature (A), salinity (B), average Chl-*a* (C) and size-fractionated chl-*a*, i.e., Chl *a*-P (pico chlorophyll), Chl *a*-N (nano chlorophyll) and Chl *a*-M (micro chlorophyll). Average concentrations of nutrients, i.e., silicates (G; SiO₃), phosphates (H; PO₄), nitrous oxides (I; NO_x), nitrite (J; NO₂), nitrate (K; NO₃) and ammonium (L; NH₄) at the WPO.

with ranges of 0.77–1.89 mD⁻¹, and lower at 0 m (1.26 ± 65 mD⁻¹), with ranges of 0.53–1.7 mD⁻¹ (Fig. 6B). Considering the water layers, the average sinking rates were higher at the SCM (1.30 mD⁻¹) than at both the MLD (1.26 mD⁻¹) and BSCM (1.27 mD⁻¹). Considering the vertical segments (Fig. 6C), the average sinking rates were found to be higher at S_{HE} (1.56 ± 0.35 mD⁻¹), especially at the BSCM (1.73 ± 0.56 mD⁻¹), than at all other sections, i.e., S_{ME} (1.51 ± 0.26 mD⁻¹), S_{NEC} (1.07 ± 0.03 mD⁻¹) and S_{KC} (1.03 ± 0.17 mD⁻¹). However, S_{ME} possessed higher vertical sinking rates at both the MLD (1.53 ± 0.26 mD⁻¹) and SCM (1.57 ± 0.22 mD⁻¹) than at the other stations (Table 1). A low sinking rate was observed at both the MLD (0.94 ± 0.2 mD⁻¹) and SCM of the Kuroshio (1.05 ± 0.14 mD⁻¹) as well as at the BSCM of the equatorial current (1.06 ± 0.3 mD⁻¹).

Environmental correlations among parameters. Correlation plots demonstrated the significant correspondences ($P < 0.05$) of TEPs and sTEP. TEP concentration showed significant negative correlations with temperature (Fig. 7). It showed positive linearity with chl-*a*, especially at 100 m depth at S_{ME} and S_{HE} (Fig. 8A). However, it maintained negative linearity with sTEP in the same zone at similar depths (Fig. 8B), which is also supported by correspondence analysis (Fig. 7). On the other hand, sTEP demonstrated significant positive correspondences ($P < 0.05$) with diatoms, cyanobacteria and Chl-*a* (Fig. 7) and negative correspondences with ammonium (Fig. 7). It also showed a highly significant negative correspondence with atmospheric pressure (Atm P) and maintained significant negative linearity ($R^2 = 0.4 \sim 0.8$) in the regression graphs, especially at 100 m of the WPO (Fig. 8C). Under the SME, sTEP showed positive linearity with cyanobacteria ($R^2 = 0.55$) at 0 m (Fig. 8D) and with diatoms ($R^2 = 0.59$) at 50 m (Fig. 8E). In this study, the TEP/Chl-*a* ratio was positively correlated ($R^2 = 0.49$) with diatoms (Fig. 8F) with high amplitudes (Fig. 9), especially at the surface (0 m) of the eddies (S_{ME} + S_{HE}).

CCA showed the close correspondence of TEP concentration with cyanobacteria abundances and nutrient concentrations (Fig. 10A). Cyanobacteria, i.e., *T. hildebrandti* and *T. theibauti* were more closely related to TEP concentration than the other dominant phytoplankton groups (Fig. 10B). Except for Chl-*a* M, the rest of the size-fractionated chl-*a* concentrations demonstrated correspondences to TEP concentration at the MLD, which may have demonstrated the resemblances of pico- and nanophytoplankton (Fig. 10C). TEP concentration

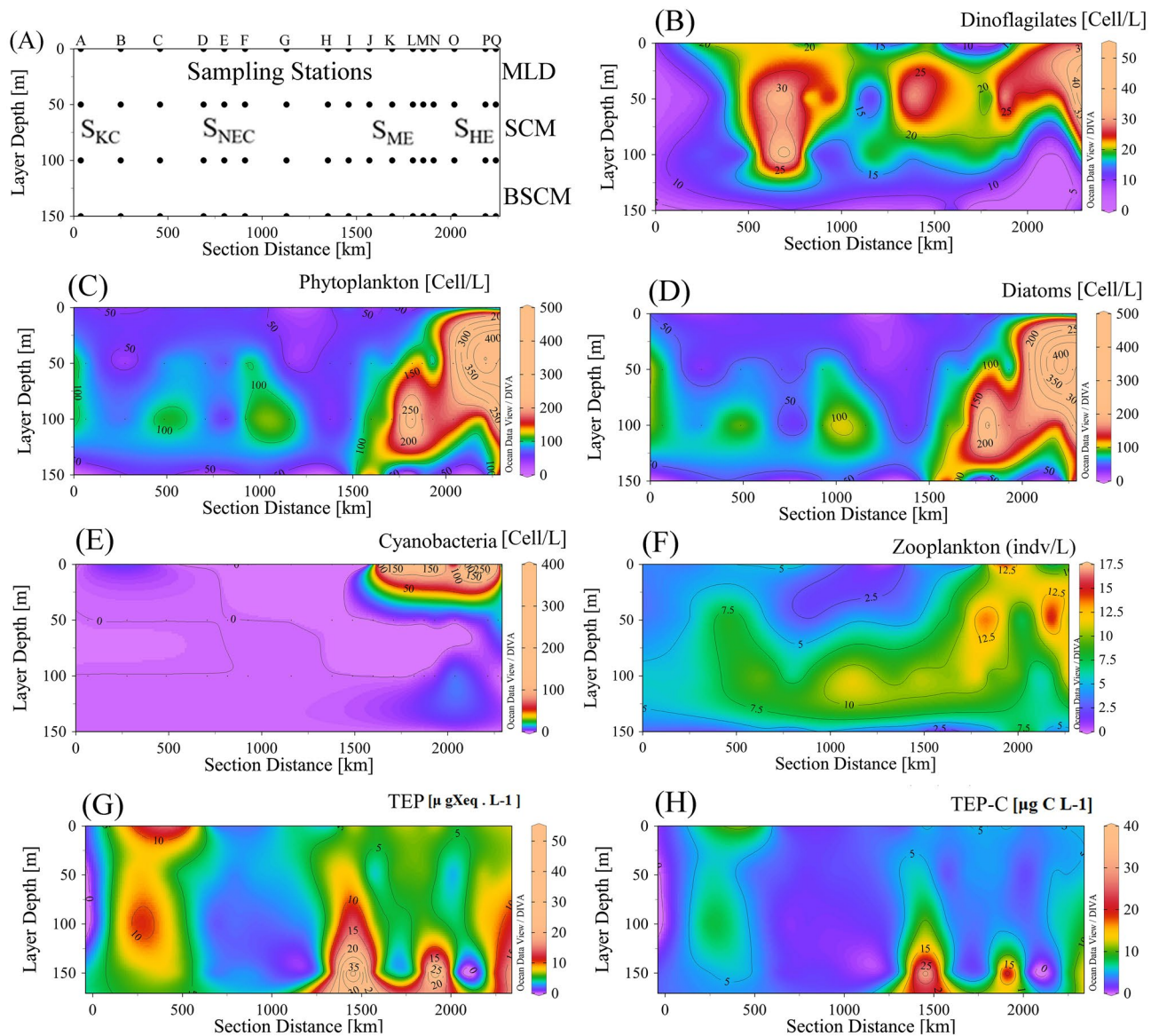


Figure 4. Segmentation of the water column, i.e., the MLD (mixed layer depth), SCM (subsurface chlorophyll maximum) and BSCM (below SCM), with station associations via geophysical forcing, i.e., S_{KC} (stations at the Kuroshio current), S_{NEC} (stations at the Northern Equatorial current), S_{ME} (stations at the Mindanao Eddy) and S_{HE} (stations at the Halmahera Eddy) throughout the study area (A) and vertical concentrations of biotic parameters, i.e., diatoms (B), dinoflagellates (C), cyanobacteria (D), TEP (E), TEP-C (F), zooplankton (G), and phytoplankton (H), in the WPO.

showed close correspondences with NH_4 contents and dinoflagellate abundances at the SCM (Fig. 10D). Only cyanobacteria demonstrated a close correspondence with TEP concentration at the BSCM (Fig. 10E) compared with other hydrobiological parameters. Using a generalized linear model (GLM), it was found that the responses of *P. alata* ($P=0.02$) and *T. theibauti* ($P=0.04$) curved positively and *T. hildebrandti* curved negatively ($P=0.03$) towards the TEP concentration (Fig. 10F).

Discussions

Hydrological stratification of study transects. The Western North Pacific (WNP) summer monsoon was identified in October⁶⁴, and boreal winter was reported between November–December³¹. Therefore, the sampling period was denoted as the transitional time of WNP weather, namely, Autumn⁶⁵. This weather is influenced by ENSO⁶⁶, which drives a critical typhoon season during WPO autumn, i.e., incidence of super typhoon Lan (category 4) on 21 October prior to the 4 days from sampling periods⁴⁵. These northwestern Pacific typhoon intensities brought up water from depths of 75 m and replaced 50% of the water of the mixed layer (30 m) through vertical mixing by wind-driven upwelling⁶⁷. Therefore, the water became well diluted between 0–150 m. These phenomena can help visualize the effects of local geophysical forces (currents, eddies) on environmental parameters across the study transect.

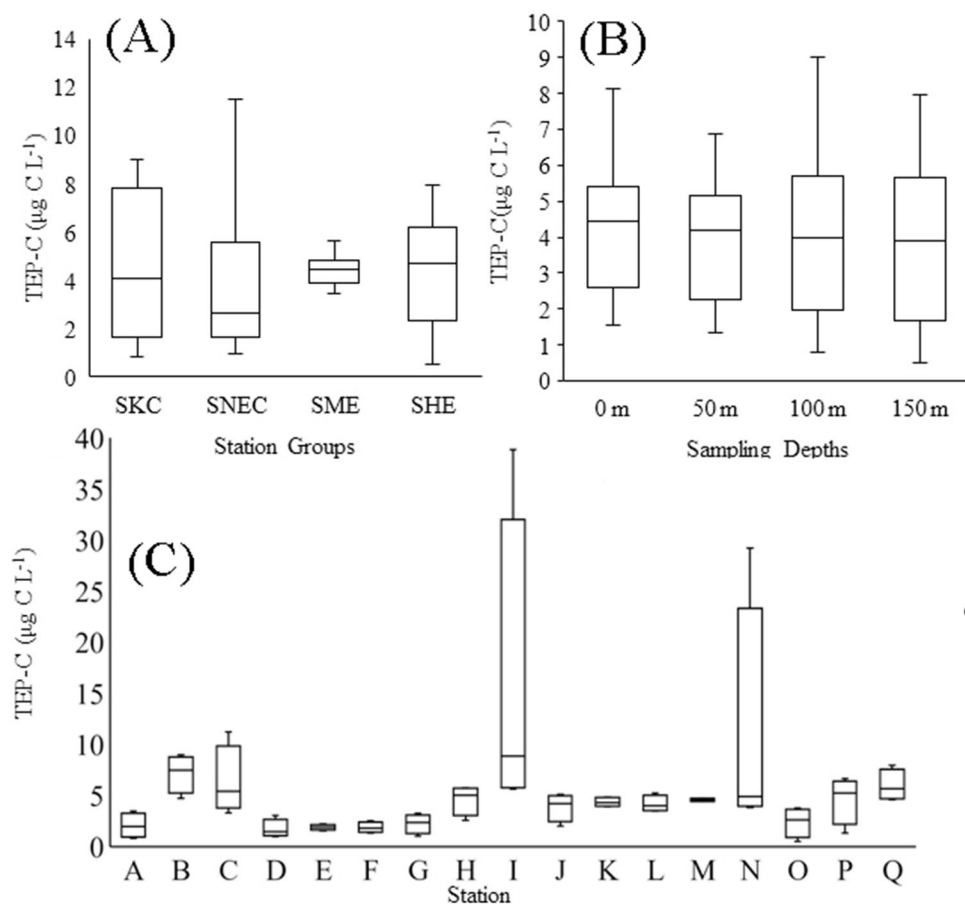


Figure 5. Average variations in TEP_C concentrations at all water depths (A) and sections (B) and at each sampling station (C) in the WPO.

Data	Water layers	Station groups				H. Ave.*
		S_{KC}	S_{NEC}	S_{ME}	S_{HE}	
TEP ($\mu\text{g Xeq. L}^{-1}$)	MLD	7.13 ± 5.21	05.27 ± 04.66	06.37 ± 00.96	6.03 ± 0.89	6.2 ± 02.9
	SCM	6.00 ± 5.41	04.98 ± 03.71	05.41 ± 01.10	6.32 ± 2.45	5.7 ± 03.2
	BSCM	5.46 ± 1.18	10.81 ± 18.26	12.29 ± 14.91	4.36 ± 5.45	8.2 ± 10.0
	V.Ave.**	6.14 ± 4.13	06.51 ± 09.59	07.37 ± 07.50	5.76 ± 2.30	6.4 ± 05.9
TEP_s (m.D^{-1})	MLD	0.94 ± 0.20	1.06 ± 0.37	1.53 ± 0.26	1.46 ± 0.24	1.2 ± 0.3
	SCM	1.05 ± 0.14	1.07 ± 0.29	1.57 ± 0.22	1.53 ± 0.30	1.3 ± 0.2
	BSCM	1.09 ± 0.26	1.06 ± 0.30	1.36 ± 0.33	1.73 ± 0.56	1.3 ± 0.4
	V.Ave.**	1.03 ± 0.17	1.07 ± 0.30	1.51 ± 0.26	1.56 ± 0.35	1.3 ± 0.3

Table 1. Variations in the average TEP concentrations and sinking rates with standard deviations across different sea regions during the study. *Horizontal average, **Vertical average.

Biogeophysical influences on TEPs

A number of statistical approaches revealed the significant relation between biogeophysical parameters and TEP concentrations during the current study. For example, salinity can influence TEP patterns¹². Here, the concentration of TEPs was dense in highly saline areas across the study transect (Fig. 2B). A positive correlation between salinity and TEP mixing intensity was also reported¹², which was observed at the MLD using CCA (Fig. 10C) during this study. On the other hand, lower salinity levels were found at the MLD than at the BSCM during the present study (Fig. 2B), which is the result of various Pacific Ocean dynamics, i.e., atmospheric convection, precipitation, and evaporation according to the literature^{68–70}. Additionally, the NEC brought less nutrient-rich water from the central Pacific⁷¹, which may cause nutrient deficiencies at S_{NEC} (Fig. 3). Furthermore, nutrient-rich water from the equatorial upwelling zone was prevented by the barrier of the northern boundary convergent front with a weak NECC under the influence of the South Equatorial current (SEC)⁷². This nutrient limitation reduced

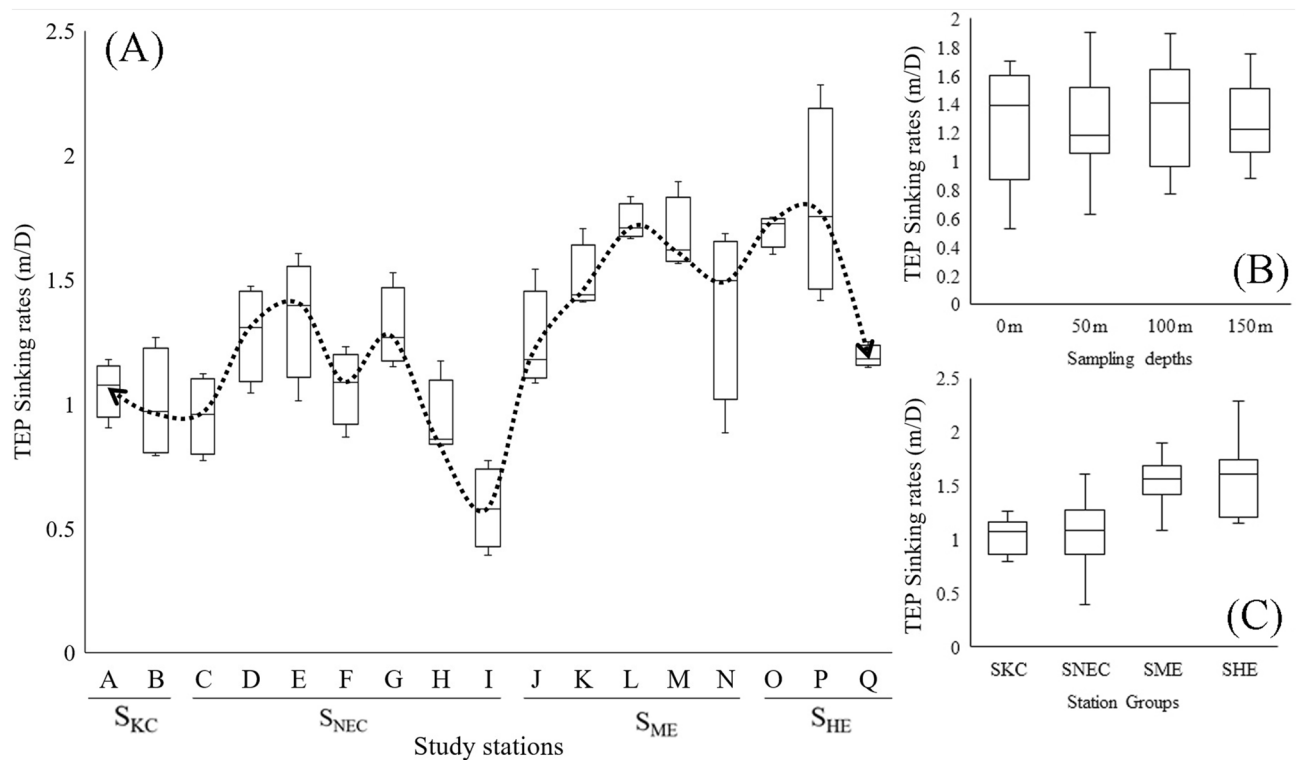


Figure 6. Average variation in sTEP through all sampling stations with line fluctuations (A) at each water depth (B) and in each section (C) in the WPO.

the biotic production⁷⁶, which may indicate a phytoplankton-derived TEP⁴ availability in the area. Notably, the downwelling feature of Halmahera⁶² combined with these local phenomena may have reduced the nutrient availability at the MLD associated with the eddies (Fig. 5). All of these oligotrophic characteristics coupled with biological phenomena may have influenced TEP depilation at the surface of the WPO.

Moderately high NO₂ and NH₄ contents were observed at the Kuroshio (Fig. 3K,L) stations, which were similar to the results of a previous study in summer (considered “before typhoon season”)⁴². This may be liable for the TEP abundances observed at KC (Fig. 4G) due to reasonable phytoplankton diversity²⁸ under the influences of nutrients from KC bifurcation from the NEC⁷³ and periodic upwelling by cyclonic typhoons⁶⁷. Phytoplankton, especially diatoms (Fig. 4D), were less abundant across the NEC⁴² due to the low nutrient supply coming from the mid Pacific⁷¹, which drives less TEP production⁴ during autumn (of this study). Cyclonic eddies brought up nutrients from the bottom layer^{74,75}, which caused phytoplankton dominance⁷⁶ at the MLD and SCM of the eddies (Fig. 3C). These relations may have induced high TEP concentrations in Mindanao (Fig. 2D), derived from phytoplankton⁴. Nitrogen-based nutrients were higher at 150 m in Mindanao (Fig. 3I), which may also be liable for the high TEP concentrations observed along this upwelling area²⁷.

Higher TEP concentration was reported in the Ross Sea (4335 $\mu\text{g Xeq L}^{-1}$) than in other reports (Table 2) due to its high nutrients and productivities⁷⁷. Considering water layers, the MLD of the Adriatic Sea and highly saline Arabian Sea demonstrated high TEP concentrations^{23,78}, among the other reported seas (Table 2). It has also been reported that seas condense with higher TEPs than straits, excluding estuaries^{79–81}. Among estuaries, the MLD of the Newson Estuary possessed a higher TEPs than others^{12,25,82}. However, across the oceans, the MLD of the WPO possessed a lower TEPs than that of the EPO²⁸ and Atlantic Ocean²⁶. Even the MLD of the northern WPO was reported to have high TEPs²⁷ compared to both the MLD and SCM of this study area due to its oligotrophic conditions and low productivities²⁰. Considering the BSCM (> 100 m), the TEP concentration was observed to be higher in the WPO than in both parts of the Mediterranean Sea^{29,83}. This study hypothesized that active downwelling forces generated by Halmahera⁶² may have brought phytoplankton groups from the surface to the BSCM. Suspended TEPs from upper layers with high sTEP ($1.73 \pm 0.56 \text{ m} \cdot \text{D}^{-1}$) can also aggregate TEPs here²⁴. Analysis also found close correspondences of cyanobacteria (Fig. 10E), i.e., *T. hildebrandti* and *T. theibauti* with TEP concentrations (Fig. 10B) in this layer. Therefore, high phytoplankton assemblages under the influence of nutrient enrichment through eddy-driven upwelling⁶¹ and cyclonic activity⁶⁷ induced a high TEP concentration at the BSCM.

Statistical correspondences of TEP. Western Pacific phytoplankton and microbial communities are controlled by nutrients^{46,84}. Therefore, phytoplankton-driven TEPs showed an average close correspondence to nutrients during the present study (Fig. 10A), which has also been found in open seas^{27,28} and polar areas⁷⁷. The surfaces of eddies and upwelling regions also influence particle distribution and organism dominance⁸⁵, which supported the correspondence of Chl-*a* with TEPs at the MLD in both CCA (Fig. 10C) and regression analysis

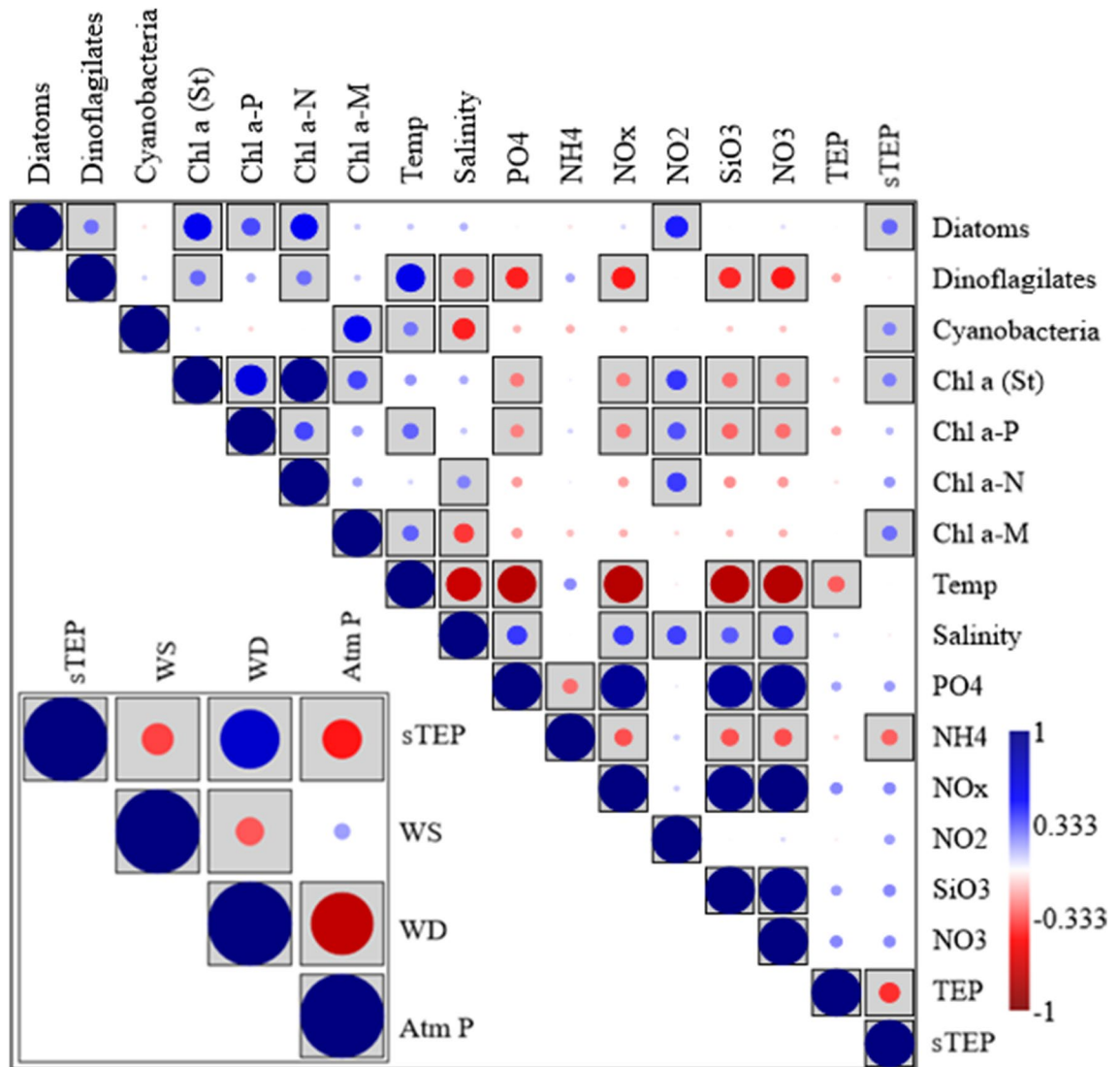


Figure 7. Correlation plots of TEPs and sTEP with other biotic and abiotic parameters after using Pearson's analysis. The gray box indicates a significant value of $P < 0.05$ (WS wind stress, WD wind direction and *Atm P* atmospheric pressure).

(Fig. 8A) of sampled data as well. Nutrient uptake by phytoplankton⁶ or nutrient upwells from the bottom^{74,75} may be influential under these scenarios.

Diatoms, especially its bloom conditions, were reported as a factor driving high concentration of TEP^{15,16,86}. In support of this, a significant positive response curve between TEPs and diatoms (Fig. 8), i.e., *P. alata*, was observed during GLM analysis (Fig. 10F). Chl-a (Fig. 8A), especially Chl-a P, showed a significant relation with TEP concentration at the MLD of the study area (Fig. 10C), which is supported by some reports on picophytoplankton, i.e., *Prochlorococcus marinus*, *Anabaena flos-aquae*¹⁷ and *Synechococcus elongatus*, which are denoted as active TEP sources⁷. On the other hand, the TEP/Chl-a ratio was negatively correlated ($R^2 = 0.49$) with diatom abundance (Fig. 8F). It was found to be higher (33.23 ± 21.46) than that observed in terrestrial areas⁸⁷ and lower than that in gulf areas²³. Additionally, diatoms showed close correspondence ($P < 0.05$) with chl-a (Fig. 7). This indicates the influence of diatoms on high TEP concentrations at areas with low chl-a abundances, which is also supported by previous reports²³. The present study observed a significant close relation of two micro cyanobacteria, i.e., *T. hildebrandti* and *T. theibauti*, with TEPs, which may act as a potential source of TEPs in the WPO⁸⁸. As an oligotrophic zone with active geophysical circulations²⁰, these phytoplankton species may have influenced TEP production across the study area. This result was also supported by a significant linear regression ($r^2 = 0.6$) between diatoms and TEP concentrations (Fig. 8E). In addition, copepods graze on TEPs^{17,18}, which may explain the TEP depletion (Fig. 4G) along zooplankton-enriched zones across the whole transect (Fig. 4F).

Biological consumption and air–water exchange also influence CO_2 exchanges in surface water⁸⁹. On this note, vertical Mindanao mixing (Fig. 1) and high plankton concentration at the MLD (Fig. 4C) may cause lower amounts of dissolved organic carbon in the surface water. In addition, an average low TEP_C was observed at the surface of the WPO (Fig. 4H). Therefore, $\text{TEP}_C\text{-CO}_2$ exchange, via bubble bursting and wave action, decreased¹⁹.

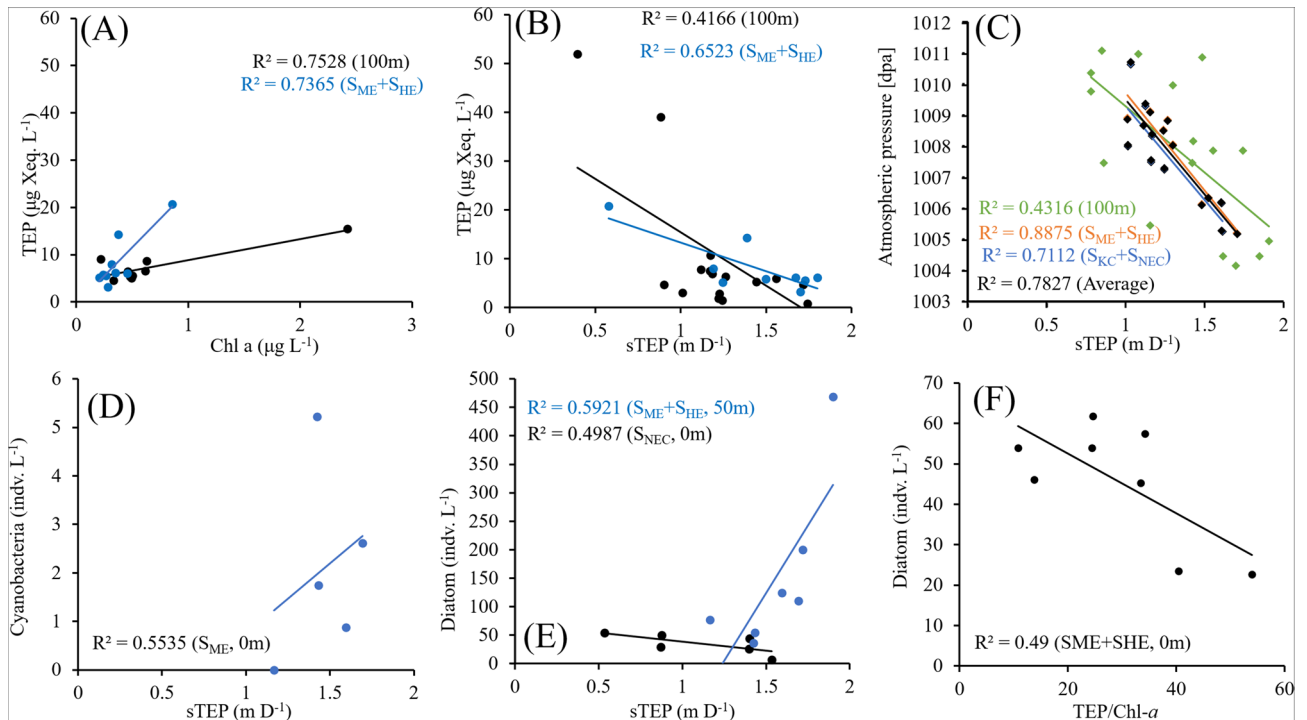


Figure 8. Significant linear regressions of diatoms, cyanobacteria, TEP, TEP/Chl-a ratio and sTEP.

A previous study suggested that TEPs should be considered in the study of particulate organic carbon (POC)²⁴ to estimate the contribution of TEPc to the carbon budget¹⁹. By obtaining averaged POC satellite data ($40 \mu\text{g L}^{-1}$) of the WPO via SatCO₂ (see supplementary file 1), this study found a 12.35% contribution of TEPc to the POC, which was considerably lower than that of the reported eutrophic zone (30%)⁹⁰. The oligotrophic condition of the WPO may be driving this scenario²⁰. Additionally, TEP sinking was revealed as an important pathway of carbon (0.02–31%) due to its significant influence ($r^2 = 0.65$) on the TEP_C (Fig. 8B), especially in eddies of WPO^{24,91,92}. Considering all these phenomena, in situ POC estimations and their relations should be considered in future research to determine the influences of TEP_C on the local carbon cycle.

Variations of TEP sinking rates. Seawater is denser than TEPs (density $0.70\text{--}0.84 \text{ g cm}^{-3}$), which indicates that pure TEPs will ascend upwards under ballast-free conditions⁹³. Therefore, the sinking rates of TEPs can be negative^{93,94}. The presence of inorganic and organic substances in seawater makes it difficult for TEPs to be pure²⁴. The sticky gel characteristic of TEPs^{95,96} may cause them to aggregate with various detrituses, particles and organisms, i.e., bacteria, phytoplankton and mineral clays⁹⁷, which carry them to downward in water¹⁹. In the WPO, high phytoplankton contents (Fig. 4C) and high TEP concentrations (Fig. 4G) at Mindanao have significant positive correlations (Fig. 8A; blue line), indicating its stickiness accordingly. This may cause the moderate sinking rates of TEPs along the ME (Table 1). However, a low TEP stickiness was also reported for increasing TEP concentrations with low downward flow^{98,99}. High TEPs with comparatively low sTEP and low phytoplankton abundances confirmed this phenomenon at the BSCM of the ME (Table 1). This result is also supported by the significant negative correlation between TEPs and sTEP (Fig. 8B). Anticlockwise ME-driven upwelling may also influence low sTEP by the physical directions of water as well⁶¹. Furthermore, cyclonic typhoons can temporarily decrease the sinking rates due to upwells of the water column from the deep sea⁶⁷. Due to its periodic activity, it can be ignored. A low phytoplankton abundance and low TEP concentrations with high sTEP were observed at the BSCM of the HE (Fig. 9B). Downwelling phenomenon of anticyclonic Halmahera may contribute to these scenarios at S_{HE} with high sinking rates⁶². Therefore, the sTEP was also influenced by characteristic of geophysical circulations and their directions in addition to the TEP influences at the WPO.

Freshwater lakes have low TEP concentrations with high sTEP (Table 3) due to the influence of phytoplankton cell aggregation¹⁰⁰. On the other hand, estuaries have also reported high sTEP via SETCOL due to high concentrations of suspended inorganic and organic particulate matter in these areas²⁴. On the other hand, the open ocean, i.e., the South Pacific Ocean, demonstrated a low sTEP due to its oligotrophic conditions⁹⁴. TEPs can be affected by variations of sTEP⁹⁰. The SETCOL method¹⁰¹ was used to measure the rate of phytoplankton sink^{102,103} as well as TEP sink^{24,93,94,104} due to its simplicity and reliability. The experiment was arranged on the deck of a sampling vessel that collected water from different depths (0–150 m) in separated plexiglass columns (Fig. 11i). It was reported that local geophysical parameters and T-S variabilities (Fig. 2A) caused differences in particle aggregation patterns (Fig. 2B) as well as sinking rates¹⁰⁵. The significant negative linearity of atmospheric pressure with the sTEP in the WPO may support those reports^{105,106} accordingly (Fig. 8C). However, the turbulence and motion of seawater were ignored in SETCOL on the deck of the sampling vessel, which may

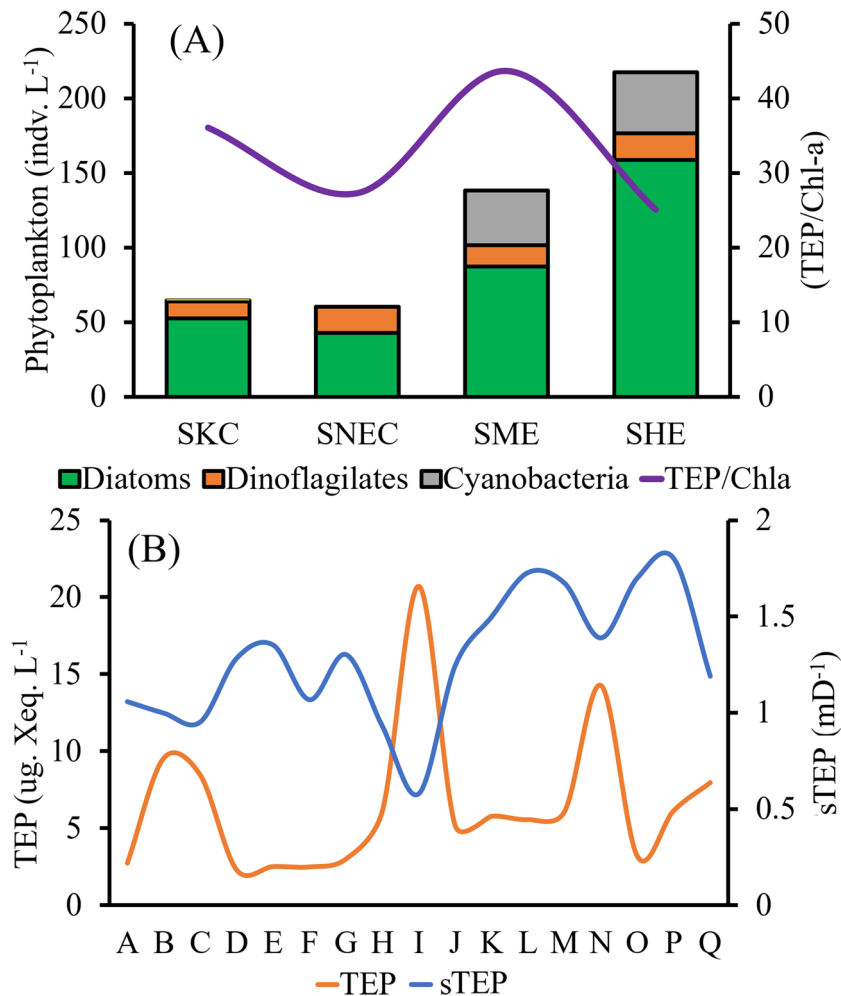


Figure 9. Average phytoplankton assemblages and patterns of TEP/Chl-*a* ratios (A) and a comparative line graph of TEP concentrations and TEPs (B) in the WPO.

have complex effects on particle sinking in the ocean^{106,107}. Therefore, this particular situation has remained undefined by theories²⁴. It was hypothesized that a high TEP concentration causes a low sTEP due to its porous aggregation structure and that a low TEP with less stickiness causes a high sTEP¹⁹. Supporting this, the present study observed low sTEP at high TEP concentrations (Fig. 9B) with a significant negative relation (Fig. 8B). All these scenarios indicate a complex relationship between TEPs and sTEP with other environmental parameters, varying from zone to zone across the WPO study transect.

Conclusions

The current study identified the TEP distribution and its relation with sTEP and other environmental parameters in the WPO. Chl-*a* significantly influenced the TEP distribution in this oligotrophic region. However, environmental differences in horizontal zones caused diatoms to alter their significant relationships with TEPs, i.e., S_{NEC} (negatively) and S_{ME} (positively). These relations indicated periodical contributions of typhoon-induced mixing at S_{NEC} and upwelling at S_{ME} . The nutrient gradient also supported these relational tangents by demonstrating inverse correspondences with zonal biotic parameters separately. On the other hand, atmospheric pressure mainly controlled the sTEP along the whole transect ($r^2 = 0.4-0.8$), which may have indirectly influenced the notable negative relation ($r^2 = 0.4-0.6$) between TEP concentrations and sTEP. During the study periods, cyanobacteria influenced the TEP increment due to nutrient upwelling, which led to low TEPs at the surface of the S_{ME} . It also contributed less to the POC spectra than to the eutrophic zone due to the general oligotrophic environment. Seasonal data collections of TEPs and sTEP can explain the more intense annual relation of particle aggregations in this oligotrophic area in the future. Additionally, the carbon contribution of TEPs under sTEP influences will become picturized more clearly by studying temporal and special variations in particle aggregations at WPOs.

Materials and methods

Study area. Water samples were taken from different depths (0, 50, 100 and 150 m) at 17 stations in the WPO (Fig. 1) from 25 October to 12 November (2017) during the Pacific typhoon season¹⁰⁸. The cruise was conducted near the equatorial area from 2° N, 130° E to 18° N, 126° E. All stations were aligned in straight-lines

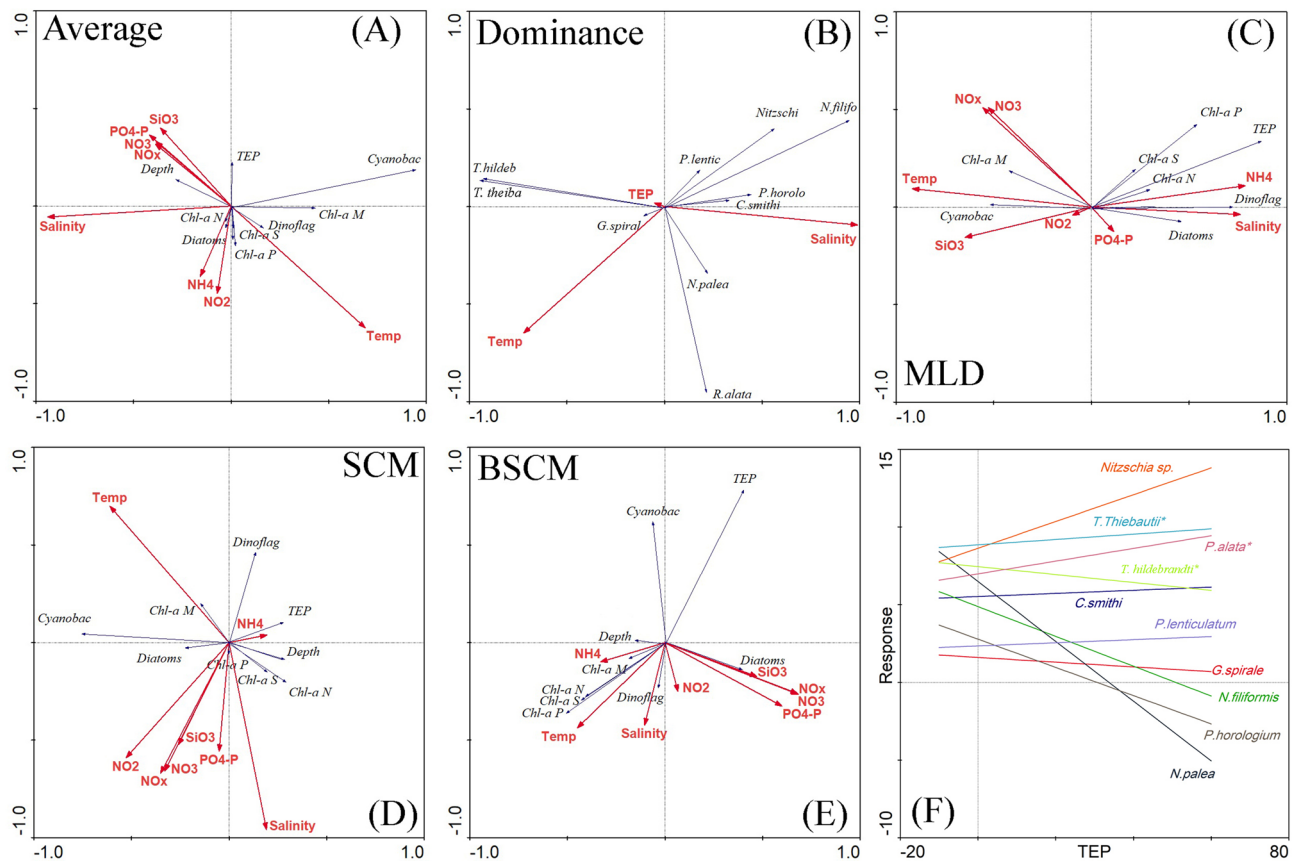


Figure 10. Canonical correspondence analysis (CCA) among different parameters on average (A) for the dominant species (B) and at different water layers, i.e., MLD (C), SCM (D) and BSCM (E) of the WPO. Response curves of species to TEPs (F) with significance levels (* = $P < 0.05$) after applying a generalized linear model (GLM).

during sampling to obtain a clear picture of the abundance in a vertically sectioned view (Fig. 4A). Sampling was performed 4 days after the super typhoon “Lan” attack⁴⁵, which experienced maximum sustained winds, reaching 250 km/h (155 mph) throughout the study area (Fig. 1).

Sample collection. A multiple rosette sampler (MRS with CTD sensors) was used to collect water from four depths (0, 50, 100 and 150 m) at each station. Samples were collected separately to measure phytoplankton abundances, Chl-*a* contents, nutrients, TEP concentrations and sTEP. In a 1 L sampling bottle, phytoplankton samples were collected with 1% formaldehyde for further analysis and identification²⁴. For Chl-*a* analysis, the collected seawater was filtered through a 25-mm GF/F and stored at $-20\text{ }^{\circ}\text{C}$ in the dark. Water samples were also taken separately to determine the concentrations of the size-fractionated Chl-*a* spectra, i.e., micro (Chl-*a* M), nano (Chl-*a* N) and pico Chl-*a* (Chl-*a* P) as supporting data. These subsamples were filtered serially through a silk net ($20\text{ }\mu\text{m} \times 20\text{ mm}$), nylon membrane ($2\text{ }\mu\text{m} \times 20\text{ mm}$) and Whatman GF/F filters ($0.7\text{ }\mu\text{m} \times 47\text{ mm}$) for size fractionated Chl-*a* analysis under a filtration vacuum with less than 100 mm Hg. Seawater from all sampling depths were directly collected in 100 mL sample bottles from MSR chambers via controlled outlets with care and stored at $-25\text{ }^{\circ}\text{C}$ for nutrient analysis.

Calculation of TEP sinking flux. Edraw Max (v9.4) was used to demonstrate the SETCOL¹⁰¹ setup on the research vessel during sampling at each study station (Fig. 11). For observation, three Plexiglass columns (Height = 0.45 m and volume = 1200 mL) for each depth were filled completely with a homogeneous water sample within 10 min after sampling, and a cover was then placed on the setup. In the vessel, the Plexiglass column was kept undisturbed for 2–3 h. A water bath (controlled thermostatically) with water jackets was placed to control the temperature by pumping water around the setup. Settled samples were collected in bottles by successive draining from the upper (A), middle (B) and bottom (C) compartments of those columns (Fig. 11i). The TEP biomass of each segment (A, B and C) from all stations was measured⁴⁴ and calculated according to the following formula:

$$\text{sTEP} = \frac{B_s}{B_t} \times \frac{L}{t}$$

	Sea/area ^(references)	Depths	TEP
		(m)	($\mu\text{g Xeq. L}^{-1}$)
Seas	The Baltic Sea ¹⁴	Surface layers	145–322
	Eastern Mediterranean Sea ⁸³	Surface layers	116–420
		50–100	48–189
		100 <	83–386
	Mediterranean Sea ²⁹	Surface layers	19.4–53.1
		50–100	9.1–94.3
		100 <	4.5–23.5
Adriatic Sea ⁷⁸	Surface layers	4–14,800	
Arabian Sea ²³	Surface layers	507–560	
Weddell Sea ¹¹⁵	Surface layers	0–48.9	
Estuaries and Bays	Jiulong River Estuary ⁸²	Surface layers	530–720
	Pearl River Estuary ²⁵	Surface layers	85–1235
	Newson Estuary ¹²	Surface layers	805–1801
	Gulf of Cadiz ¹¹⁶	Surface layers	25–717
	Gulf of Aqaba ¹¹⁷	Surface layers	130–222
		50–100	106–228
		100 <	23–209
	Chesapeake Bay ¹¹⁸	Surface layers	37–2820
Santa Barbara Low Strait ⁴³	Surface layers	85–252	
Oceans	Western tropical North Pacific ²⁷	Surface layers	43.3
		50–100	42.2
	Eastern tropical North Pacific ²⁸	Surface layers	22.5
		50–100	9.2
	Eastern subarctic North Atlantic ²⁶	Surface layers	20–60
	Eastern subarctic North Pacific ²⁸	Surface layers	28.7
		50–100	11.6
	Western subarctic North Pacific ¹¹⁹	Surface layers	40–190
	Western Pacific Ocean (This Study)	Surface layers	2.06–14.94
50–100		1.08–15.33	
100 <		0.69–51.80	

Table 2. TEPs in different layers of various waterbodies from different studies.

Location	TEP _s (m d ⁻¹)	Method
Santa Barbara strait ⁹³	–0.22–0.04	SETCOL
South Pacific Ocean ⁹⁴	–0.29 ~ 0.49	SETCOL
Quéntar Lake ¹⁰⁴	1.12 ~ 1.31	Sediment trap
Changjiang Estuary ²⁴	0.08–1.08	SETCOL
Western Pacific Ocean (This Study)	0.30–2.28	SETCOL

Table 3. Variations in TEP_s and applied methods from different reports.

where sTEP is the sinking rate of TEPs; B_s is the biomass of TEPs settled into the bottom compartment; B_t is the total biomass of TEPs in the column; L is the length of the column; and t is the settling interval. Samples from all depths were triplicated during measurement for better data analysis and marked according to stations for both sTEP and TEPs.

TEP examination. Samples of TEPs were measured according to the dye-binding method using xanthan gum⁴³. A 50–100 mL sample was taken each time (6 replicates) during the colorimetric method after ensuring a xanthan gum curve (fx; as the mean) using absorption measurements. Fifty milliliters (V_f) of sea water was constantly filtered using a low-pressure (Fig. 11ii) vacuum (150 mm of Hg) using polycarbonate filters (0.4- μm pore-size). Afterwards, particle dyeing was performed on the filter for ~ 2 s with 500 μL of a 0.02% aqueous solution of Alcian blue (8 GX) in 0.06% acetic acid (pH 2.5). After staining, the filters were rinsed once with distilled water to remove excess dye. Rinsing does not wash off the dye as it binds with substrates⁴³. Filters were then transferred into 25-mL beakers with 6 mL of 80% sulfuric acid and soaked for 2 h. The beakers were gently

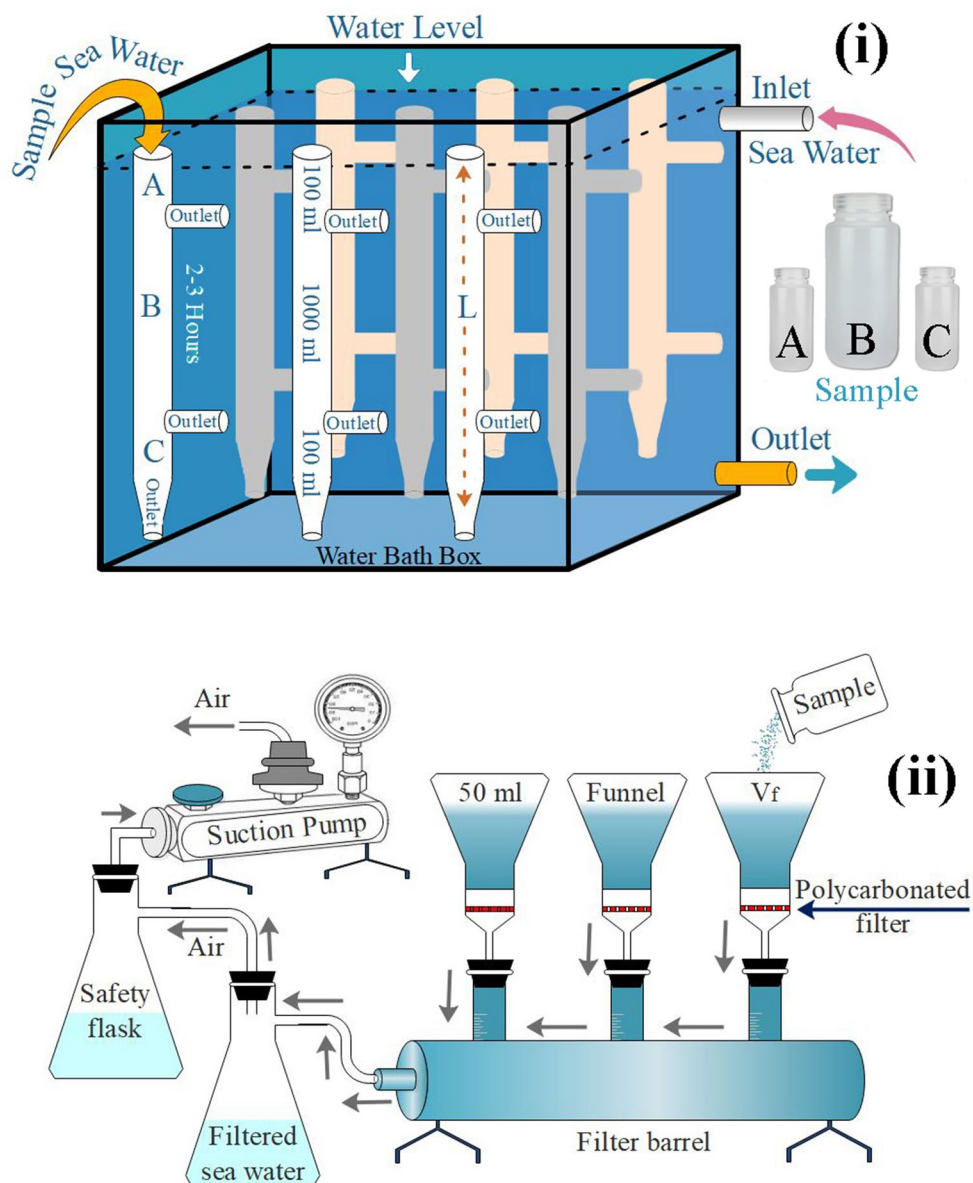


Figure 11. SETCOL setup (A) of the vessel and batch filtration processes of colloidal TEP (B) according to the literature (Drawn by Dr. M Shahanul Islam, 1st author).

agitated 3–5 times during this period. The maximum absorption of the solution (E_{787}) lies at 787 nm, and absorption was observed using a 1-cm cuvette against distilled water (B_{787}) as a reference. The equation was as follows:

$$TEP = (E_{787} - B_{787}) \times (V_f)^{-1} \times f_x.$$

The average calibration factor of xanthan gum (f_x) was measured (9.83) using a regression plot after calculating several absorptions from 0.3–3 ml colloidal free solutions⁴³. Carbon contents associated with the TEP concentration (TEP_C , $\mu\text{g C L}^{-1}$) were calculated after finalizing with the slope (0.75) from the equation as follows⁴⁴:

$$TEP_C = 0.75 \times TEP_{color}$$

where TEP_{color} is the TEP concentration²⁴ in units of $\mu\text{g Xeq L}^{-1}$.

Measurement of environmental parameters. Temperature and salinity were recorded from different depths by CTD sensors while sampling from the study area. Nutrient (NO_x , NH_4 , NO_3^- , NO_2^- , PO_4 and SiO_3) analysis was performed by a fully automated (SANPLUS, Dutch SKALAR company) wet chemical analyzer¹⁰⁹. Samples of phytoplankton (1 L, preserved with 1% formaldehyde) were analyzed according to modified Uter-

möhl methods¹¹⁰ under an inverted microscope after settling for 24 h. The dominance index was used to describe phytoplankton-dominant species using the following equation:

$$Y = \frac{n_i}{N} \times f_i.$$

where N is the total cell abundance of all species, n_i is the total cell of species i and f_i is the count of occurrences of species i in all samples¹¹¹. Chl-*a* was measured from sample water using a fluorescence method in the laboratory after soaking in 90% acetone¹¹². The filters were placed into 20-mL glass tubes, and the pigments were then extracted with 5 mL of 90% acetone and stored in the dark at 4 °C for 24 h. After standard calibration, a Turner-Designs Trilogy™ fluorometer was used for chl-*a* measurement.

Data analysis. Sampling transects were categorized by KC-, NEC-, Mindanao- and Halmahera-controlled water masses in three different layers, i.e., MLD, SCM and below SCM (BSCM). The stations were distributed accordingly (S_{KC} , S_{NEC} , S_{ME} and S_{HE}). After tabulation of the data, various multivariate analyses were performed. Surfer (version 12) was used for the average surface demonstration of all recorded and examined parameters. The concentrations of different parameters were shown using line graphs in Excel stats software and contour color maps in the Ocean Data View (ODV 2018). Particulate organic carbon (POC) data (supplementary file 1) were downloaded from the WGS-84 SOA (Second Institute of Oceanography database). A supplementary color map was produced using SatCO₂ software (V 3.0) with the SOA data (File name: NASA_MODIS_MODIS_20171101TO20171130_L3B_GLOBAL_9km_POC_V2017_2020_01_31_15_56_39_High). Cluster analysis (MCA) was performed after using the Pearson coefficient in Multivariate Statistical Package software¹¹³. Linear regressions were performed using Microsoft Excel (v2016) software. SPSS (v25) was used for Pearson's correlation and covariance analyses. Past (v3) software was used to demonstrate the Pearson correlation as graphical plots. Canonical correspondence analysis (CCA) and generalized linear model (GLM) were performed by Canoco software¹¹⁴ (version 4.14). Focused sTEP and TEPs data were tested through linear regression against each environmental parameter in Origin Pro (v6). However, data were demonstrated in graphs on the basis of significant relationship accordingly.

Received: 13 June 2019; Accepted: 16 March 2021

Published online: 31 May 2021

References

- Allredge, A. L., Passow, U. & Logan, B. E. The abundance and significance of a class of large, transparent organic particles in the ocean. *Deep-Sea Res.* **I**(40), 1131–1140 (1993).
- Kraus, M. Zur Bildung von TEP (Transparent Exopolymer Particles) in der Kieler Bucht. Diplom Christian-Albrechts-Universität Kiel Planktologie Kiel (1997)
- Mopper, K. *et al.* Role of surface-active carbohydrates in the flocculation of a diatom bloom in a mesocosm. *Deep-Sea Res.* **II**(42), 47–73 (1995).
- Passow, U. Transparent exopolymer particles (TEP) in aquatic environments. *Prog. Oceanogr.* **55**, 287–333 (2002).
- Williams, P. J. The importance of losses during microbial growth, commentary on the physiology, measurement, and ecology of the release of dissolved organic material. *Mar. Microb. Food Webs* **4**, 175–206 (1990).
- Staats, N., Stal, L. J. & Mur, R. L. Exopolysaccharide production by the epipelagic diatom *Cylindrotheca closterium*, effects of nutrient conditions. *J. Exp. Mar. Biol. Ecol.* **249**, 13–27 (2000).
- Berman-Frank, I., Rosenberg, G., Levitan, O., Haramaty, L. & Mari, X. Coupling between autocatalytic cell death and transparent exopolymeric particle production in the marine cyanobacterium *Trichodesmium*. *Environ. Microbiol.* **9**, 1415–1422 (2007).
- Mari, X. & Burd, A. B. Seasonal size spectra of transparent exopolymeric particles (TEP) in a coastal sea and comparison with those predicted using coagulation theory. *Mar. Ecol. Progr. Ser.* **163**, 63–76 (1998).
- Engel, A. Bildung und Zusammensetzung und Sinkgeschwindigkeiten Marine Aggregate. Phd. Thesis Christian-Albrechts-Universität Kiel Institut für Meereskunde Kiel (1998)
- Engel, A. *et al.* Transparent exopolymer particles and dissolved organic carbon production by *Emiliania huxleyi* exposed to different CO₂ concentrations, a mesocosm experiment. *Aquat. Microb. Ecol.* **34**, 93–104 (2004).
- Sun, C. C. *et al.* Distribution characteristics of the transparent exopolymer particle in the Pearl River Estuary. *China. J. Geophys. Res.* **117**, 2 (2012).
- Wetz, M. S., Robbins, M. C. & Paerl, H. W. Transparent exopolymer particles (TEP) in a river-dominated estuary, spatial and temporal distributions and an assessment of controls upon TEP formation. *Estuaries Coasts* **32**, 447–455 (2009).
- Mari, X. *et al.* Aggregation dynamics along a salinity gradient in the Bach Dang estuary, North Vietnam. *Estuar. Coast. Shelf Sci.* **96**, 151–158 (2012).
- Engel, A. Direct relationship between CO₂ uptake and transparent exopolymer particles production in natural phytoplankton. *J. Plankton Res.* **24**, 49–53 (2002).
- Fukao, T., Kimoto, K. & Kotani, Y. Effect of temperature on cell growth and production of transparent exopolymer particles by the diatom *Coscinodiscus granii* isolated from marine mucilage. *J. Appl. Phycol.* **24**, 181–186 (2012).
- Galgani, L. & Engel, A. Accumulation of gel particles in the sea-surface microlayer during an experimental study with the diatom *Thalassiosira weissflogii*. *Int. J. Geosci.* **4**, 129–145 (2013).
- Surosz, W., Palinska, K. A. & Rutkowska, A. Production of transparent exopolymer particles (TEP) in the nitrogen fixing *Cyanobacterium Anabaena flos-aquae* Ol-K10. *Oceanologia* **48**, 385–394 (2006).
- Passow, U. & Allredge, A. L. Do transparent exopolymer particles (TEP) inhibit grazing by the euphausiid *Euphausia pacifica*. *J. Plankton Res.* **21**, 2203–2217 (1999).
- Mari, X., Passow, U., Migon, C., Burd, A. B. & Legendre, L. Transparent exopolymer particles, effects on carbon cycling in the ocean. *Prog. Oceanogr.* **151**, 13–37 (2017).
- Everett, J. D., Baird, M. E., Roughan, M., Suthers, I. M. & Dublin, M. A. Relative impact of seasonal and oceanographic drivers on surface chlorophyll *a* along a Western boundary current. *Prog. Oceanogr.* **120**, 340–351 (2014).

21. Christian, J. R., Murtugudde, R., Ballabrera-Poy, J. & McClain, C. R. A ribbon of dark water, phytoplankton blooms in the meanders of the Pacific North Equatorial Countercurrent. *Deep Sea Res. Part II* **51**, 209–228 (2004).
22. Ramaiah, N., Yoshikawa, T. & Furuya, K. Temporal variations in transparent exopolymer particles (TEP) associated with a diatom spring bloom in a subarctic ria in Japan. *Mar. Ecol. Progr. Ser.* **212**, 79–88 (2001).
23. Prieto, L. *et al.* Distribution of TEP in the euphotic and upper mesopelagic zones of the southern Iberian coasts. *Deep-Sea Res.* **II**(53), 1314–1328 (2006).
24. Guo, S. & Sun, J. Sinking Rates and Export Flux of Transparent Exopolymer Particles (TEPs) in a Eutrophic Coastal Sea, A Case Study in the Changjiang (Yangtze River) Estuary. *bioRxiv* 357053 (2018)
25. Sun, C. C. *et al.* Distribution of transparent exopolymer particles in the Pearl River estuary in Summer. *J. Top. Oceanogr.* **29**, 81–87 (2010).
26. Engel, A. Distribution of transparent exopolymer particles (TEP) in the northeast Atlantic Ocean and their potential significance for aggregation processes. *Deep-Sea Res.* **I**(51), 83–92 (2004).
27. Kodama, T. *et al.* Vertical distribution of transparent exopolymer particle (TEP) concentration in the oligotrophic western tropical North Pacific. *Mar. Ecol. Progr. Ser.* **513**, 29–37 (2014).
28. Wurl, O., Miller, L. & Vagle, S. Production and fate of transparent exopolymer particles in the ocean. *J. Geophys. Res. Oceans* **116**, 13 (2011).
29. Ortega-Retuerta, E., Duarte, C. M. & Reche, I. Significance of bacterial activity for the distribution and dynamics of transparent exopolymer particles in the Mediterranean Sea. *Microb. Ecol.* **59**, 808–818 (2010).
30. Verdugo, P. *et al.* The oceanic gel phase, a bridge in the DOM-POM continuum. *Mar. Chem.* **92**, 67–85 (2004).
31. Hu, D. X. *et al.* Pacific western boundary currents and their roles in climate. *Nature* **522**, 299–308 (2015).
32. Canini, N. D. & Metillo, E. B. Temporal changes in the community structure of phytoplankton in Panguil Bay, Philippine mangrove estuary. *ACL Bioflux* **10**, 410–420 (2017).
33. Azanza, R. V., David, L. T., Borja, R. T., Baula, I. U. & Fukuyo, Y. An extensive *Cochlodinium* bloom along the western coast of Palawan Philippines. *Harmful Algae* **7**, 324–330 (2008).
34. Angara, E. V. *et al.* Diversity and abundance of phytoplankton in Casiguran waters, Aurora Province, Central Luzon Northern Philippines. *ACL Bioflux* **6**, 358–377 (2013).
35. Asis, J. J. C., Campos, W. L. & Nabuab, F. M. Abundance, composition and distribution of phytoplankton in Calamianes Palawan. *Sci. Dil.* **18**, 1–9 (2006).
36. Loder, J. W., Boicourt, W. C. & Simpson, J. H. Western ocean boundary shelves, coastal segment, in *The Sea*. In *The global coastal ocean, regional studies and syntheses* (eds Brink, K. H. & Robinson, A. R.) 3–27 (John Wiley, 1998).
37. Koslow, J. A. *et al.* The effect of the Leeuwin current on phytoplankton biomass and production off Southwestern Australia. *J. Geophys. Res. Oceans* **113**, C07050 (2008).
38. Zhou, H., Yuan, D., Guo, P., Shi, M. & Zhang, Q. Meso-scale circulation at the intermediate-depth east of Mindanao observed by Argo profiling floats. *China Earth Sci.* **53**, 432–440 (2010).
39. Zhang, Q., Liu, H., Zhou, H. & Zheng, D. Variation features of the Mindanao eddy from Argo data. *Atmos. Ocean* **50**, 103–115 (2012).
40. Rodríguez, J. M., Hernández-León, S. & Barton, E. D. Mesoscale distribution of fish larvae in relation to an upwelling filament off Northwest Africa. *Deep Sea Res. Part I Oceanogr. Res. Pap.* **46**, 1969–1984 (1999).
41. Okazaki, Y., Nakata, H. & Kimura, S. Effects of frontal eddies on the distribution and food availability of anchovy larvae in the Kuroshio Extension. *Mar. Freshw. Res.* **53**, 403–410 (2002).
42. Chen, Y., Sun, X. & Zhun, M. Net-phytoplankton communities in the western boundary currents and their environmental correlations. *J. Oceanol. Limnol.* **36**, 305–316 (2018).
43. Passow, U. & Alldredge, A. L. A dye-binding assay for the spectrophotometric measurement of transparent exopolymer particles (TEP). *Limnol. Oceanogr.* **40**, 1326–1335 (1995).
44. Engel, A. & Passow, U. Carbon and nitrogen content of transparent exopolymer particles (TEP) in relation to their Alcian Blue adsorption. *Mar. Ecol. Progr. Ser.* **219**, 1–10 (2001).
45. Kitamoto, Asanobu. Typhoon List by Wind Information. Digital Typhoon. Japan Meteorological Agency. Retrieved October 23, 2017.
46. Li, B., Yuan, D. & Zhou, H. Water masses in the far western equatorial Pacific during the winters of 2010 and 2012. *J. Oceanol. Limnol.* **36**, 1459–1474 (2018).
47. Cannon, G. A. Tropical waters in the western Pacific Ocean, August–September 1957. *Deep Sea Res. Oceanogr. Abstracts* **13**, 1139–1148 (1966).
48. Tsuchiya, M. Upper waters of the intertropical Pacific Ocean. In *Johns Hopkins Oceanographic Studies*. No. 4. The Johns Hopkins Press, Baltimore (1968)
49. Hasunuma, K. Formation of the intermediate salinity minimum in the northwestern Pacific Ocean. *Bull. Ocean Res. Inst. Univ. Tokyo* **9**, 1–47 (1978).
50. Talley, L. D. Distribution and formation of North Pacific Intermediate Water. *J. Phys. Oceanogr.* **23**, 517–537 (1993).
51. Wang, F., Li, Y. L., Zhang, Y. H. & Hu, D. X. The subsurface water in the North Pacific tropical gyre. *Deep Sea Res. Part I* **75**, 78–92 (2013).
52. Lindstrom, E. *et al.* The western equatorial Pacific Ocean circulation study. *Nature* **330**, 533–537 (1987).
53. Tsuchiya, M., Lukas, R., Fine, R. A., Firing, E. & Lindstrom, E. Source waters of the Pacific equatorial undercurrent. *Prog. Oceanogr.* **23**, 101–147 (1989).
54. Tsuchiya, M. Flow path of the antarctic intermediate water in the western equatorial south Pacific ocean. *Deep Sea Res. Part A Oceanogr. Res. Pap.* **38**, S273–S279 (1991).
55. Fine, R. A., Lukas, R., Bingham, F. M., Warner, M. J. & Gammon, R. H. The western equatorial Pacific, A water mass crossroads. *J. Geophys. Res.* **99**, 25063–25080 (1994).
56. Qu, T. D. & Lindstrom, E. J. Northward intrusion of Antarctic Intermediate Water in the western Pacific. *J. Phys. Oceanogr.* **34**, 104–118 (2004).
57. Delcroix, T. & Hénin, C. Seasonal and interannual variations of sea surface salinity in the tropical Pacific Ocean. *J. Geophys. Res.* **96**, 135–150 (1991).
58. Chen, Y. *et al.* Spatial variability of phytoplankton in the Pacific western boundary currents during summer 2014. *Mar. Freshw. Res.* **68**, 1887–1900 (2017).
59. Suzuki, T. *et al.* Seasonal cycle of the Mindanao Dome in the CCSR/NIES/FRCGC atmosphere-ocean coupled model. *Geophys. Res. Lett.* **32**, L17604 (2005).
60. Qiu, B. & Joyce, T. M. Interannual variability in the mid- and low-latitude western North Pacific. *J. Phys. Oceanogr.* **22**, 1062–1079 (1992).
61. Kashino, Y., Ishida, A. & Hosoda, S. Observed ocean variability in the Mindanao dome region. *J. Phys. Oceanogr.* **41**, 287–302 (2011).
62. Kashino, Y., Atmadipoera, A., Kuroda, Y. & Lukijanto, H. Observed features of the Halmahera and Mindanao Eddies. *J. Geophys. Res. Oceans* **118**, 6543–6560 (2013).

63. Masumoto, Y. & Yamagata, T. Response of the western tropical Pacific to the Asian winter monsoon, The generation of the Mindanao Dome. *J. Phys. Oceanogr.* **21**, 1386–1398 (1991).
64. Chou, C., Tu, J. Y. & Yu, J. Y. Interannual variability of the Western North Pacific summer Monsoon, differences between ENSO and Non-ENSO years. *J. Clim.* **16**, 2275–2287 (2003).
65. Tsou, C. H., Hsu, H. H. & Hsu, P. C. The role of multiscale interaction in synoptic-scale eddy kinetic energy over the western north pacific in autumn. *J. Clim.* **27**, 3750–3766 (2014).
66. Ding, R. *et al.* Influences of the north pacific Victoria mode on the south china sea summer monsoon. *Atmosphere* **9**, 229 (2018).
67. Mei, W., Xie, S. P., Primeau, F., McWilliams, J. C. & Pasquero, C. Northwestern Pacific typhoon intensity controlled by changes in ocean temperatures. *Sci. Adv.* **1**, e1500014–e1500014 (2015).
68. Levitus, S. & Boyer, T. P. World Ocean Atlas 1994 Vol. 3, Salinity (NOAA Atlas NESDIS, US Department of Commerce, Washington DC, (1994)
69. Cronin, M. F. & McPhaden, M. J. Upper ocean salinity balance in the western equatorial Pacific. *J. Geophys. Res.* **103**, 27567–27587 (1998).
70. Stott, L. *et al.* Decline of surface temperature and salinity in the western tropical Pacific Ocean in the Holocene epoch. *Nature* **431**, 56–59 (2004).
71. Eldin, G. & Rodier, M. Ocean physics and nutrient fields along 180 degrees during an El Niño–Southern Oscillation cold phase. *J. Geophys. Res.* **108**, 8137 (2003).
72. Feely, R. A. *et al.* Seasonal and interannual variability of CO₂ in the equatorial Pacific. *Deep Sea Res. Part II*(49), 2443–2469 (2002).
73. Robidart, J. C., Magasin, J. D., Shilova, I. N., Turk-Kubo, K. A., Wilson, S. T., Karl, D. M. *et al.* Effects of nutrient enrichment on surface microbial community gene expression in the oligotrophic North Pacific Subtropical Gyre. *ISME J.* (2018)
74. Johnson, K. S., Riser, S. C. & Karl, D. M. Nitrate supply from deep to near-surface waters of the North Pacific Subtropical Gyre. *Nature* **465**, 1062–1065 (2010).
75. Mahaffey, C., Björkman, K. M. & Karl, D. M. Phytoplankton response to deep seawater nutrient addition in the North Pacific Subtropical Gyre. *Mar. Ecol. Progr. Ser.* **460**, 13–34 (2012).
76. Jin, J. *et al.* Nutrient dynamics and coupling with phytoplankton species composition during the spring blooms in the Yellow Sea. *Deep Sea Res. Part II* **97**, 16–32 (2013).
77. Hong, Y., Smith, W. O. Jr. & White, A. M. Studies on transparent exopolymer particles (TEP) produced in the Ross sea (Antarctica) and by *phaeocystis Antarctica (prymnesiophyceae)*. *J. Phycol.* **33**, 368–376 (1997).
78. Radic, T. *et al.* Transparent exopolymeric particles' distribution in the northern Adriatic and their relation to microphytoplankton biomass and composition. *Sci. Total Environ.* **353**, 151–161 (2005).
79. Lili, M. A., Chen, M., Guo, L., Lin, F. & Tong, J. Distribution and source of transparent exopolymer particles in the northern bering sea. *ActaOceanol. Sin.* **34**, 81–90 (2012).
80. Corzo, A. *et al.* Spatial distribution of transparent exopolymer particles in the Bransfield Strait Antarctica. *J. Plankton Res.* **27**, 635–646 (2005).
81. Shu, Y., Zhang, G. & Sun, J. The distribution and origin of transparent exopolymer particles at the PN section in the East China Sea. *Haiyang Xuebao.* **40**, 110–119 (2018).
82. Peng, A. & Huang, Y. Study on TEP and its relationships with uranium, thorium, polonium isotopes in Jiulong Estuary. *J. Xiamen Univ. (Nat. Sci.)* **46**, 38–42 (2007).
83. Bar-Zeev, E. *et al.* Transparent exopolymer particle (TEP) dynamics in the eastern Mediterranean Sea. *Mar. Ecol. Progr. Ser.* **431**, 107–118 (2011).
84. Rii, Y. M., Bidigare, R. R. & Church, M. J. Differential responses of eukaryotic phytoplankton to nitrogenous nutrients in the north pacific subtropical Gyre. *Front. Mar. Sci.* **5**, 2 (2018).
85. Chen, C. C., Kwo, S. F., Chung, S. W. & Liu, K. K. Winter phytoplankton blooms in the shallow mixed layer of the South China Sea enhanced by upwelling. *J. Mar. Syst.* **59**, 97–110 (2006).
86. Mari, X. Carbon content and C:N ratio of transparent exopolymeric particles (TEP) produced by bubbling exudates of diatoms. *Mar. Ecol. Progr. Ser.* **183**, 59–71 (1999).
87. Chowdhury, C., Majumder, N. & Jana, T. K. Seasonal distribution and correlates of transparent exopolymer particles (TEP) in the waters surrounding mangroves in the Sundarbans. *J. Sea Res.* **112**, 65–74 (2016).
88. Xue, B., Sun, J. & Li, T. Phytoplankton community structure of northern South China Sea in summer of 2014 (in Chinese). *ActaOceanol. Sin.* **38**, 54–65 (2016).
89. Dandonneau, Y. Sea surface partial pressure of carbon dioxide in the eastern Equatorial Pacific (August 1991 to October 1992)—A multivariate analysis of physical and biological factors. *Deep Sea Res. Part II*(42), 349–364 (1995).
90. Passow, U. *et al.* The origin of transparent exopolymer particles (TEP) and their role in the sedimentation of particulate matter. *Cont. Shelf Res.* **21**, 327–346 (2001).
91. Stoderegger, K. E. & Herndl, G. J. Production of exopolymer particles by marine bacterioplankton under contrasting turbulence conditions. *Mar. Ecol. Progr. Ser.* **189**, 9–16 (1999).
92. Obernosterer, I. & Herndl, G. J. Phytoplankton extracellular release and bacterial growth, dependence on the inorganic N P ratio. *Mar. Ecol. Progr. Ser.* **116**, 247–257 (1995).
93. Azetsu-Scott, K. & Passow, U. Ascending marine particles, significance of transparent exopolymer particles (TEP) in the upper ocean. *Limnol. Oceanogr.* **49**, 741–748 (2004).
94. Mari, X. Does ocean acidification induce an upward flux of marine aggregates?. *Biogeosciences* **5**, 1023–1031 (2008).
95. Engel, A. The role of transparent exopolymer particles (TEP) in the increase in apparent particle stickiness (a) during the decline of a diatom bloom. *J. Plankton Res.* **22**, 485–497 (2000).
96. Rochelle-Newall, E., Mari, X. & Pringault, O. Sticking properties of transparent exopolymeric particles (TEP) during aging and biodegradation. *J. Plankton Res.* **32**, 1433–1442 (2010).
97. Prieto, L. *et al.* Scales and processes in the aggregation of diatom blooms, high time resolution and wide size range records in a mesocosm study. *Deep-Sea Res. II*(49), 1233–1253 (2002).
98. Kjørboe, T. *et al.* Intensive aggregate formation with low vertical flux during an upwelling induced diatom bloom. *Limnol. Oceanogr.* **43**, 104–116 (1998).
99. Mari, X. & Robert, M. Metal induced variations of TEP sticking properties in the southwestern lagoon of New Caledonia. *Mar. Chem.* **110**, 98–108 (2008).
100. Vicente, I. D., Ortega-Retuerta, E., Romera, O., Moreles-Baquero, R. & Reche, I. Contribution of transparent exopolymer particles to carbon sinking flux in an oligotrophic reservoir. *Biogeochemistry* **96**, 13–23 (2009).
101. Bienfang, P. K. SETCOL—a technologically simple and reliable method for measuring phytoplankton sinking rates. *Can. J. Fish. Aquat. Sci.* **38**, 1289–1294 (1981).
102. Guo, S. *et al.* Sinking rates of phytoplankton in the Changjiang (Yangtze River) estuary, A comparative study between *Prorocentrum dentatum* and *Skeletonema dornhii* bloom. *J. Mar. Syst.* **154**, 5–14 (2016).
103. Riebesell, U. Comparison of sinking and sedimentation rate measurements in a diatom winter/spring bloom. *Mar. Ecol. Progr. Ser.* **54**, 109–119 (1989).

104. Vicente, I. D. & Retuerta, E. O. Contribution of transparent exopolymer particles to carbon sinking flux in an oligotrophic reservoir. *Biogeochemistry* **96**, 13–23 (2009).
105. Dunne, J., Armstrong, R., Gnanadesikan, A. & Sarmiento, J. Empirical and mechanistic models for the particle export ratio. *Glob. Biogeochem. Cycles* **19**, 2 (2005).
106. Javier, R., Carlos, M. G. & Jaime, R. Sedimentation loss of phytoplankton cells from the mixed layer, effects of turbulence levels. *J. Plankton Res.* **18**, 1727–1734 (1996).
107. Ruiz, J., Macias, D. & Peters, F. Turbulence increases the average settling velocity of phytoplankton cells. *Proc. Natl. Acad. Sci. U.S.A.* **101**, 17720–17724 (2004).
108. Hodge, W. Characteristics of North Pacific Typhoons. *OCEANS* **76** (1976)
109. Liu, S. M. *et al.* The impact of anthropogenic activities on nutrient dynamics in the tropical Wenchanghe and Wenjiaohe Estuary and Lagoon system in East Hainan. *China. Mar. Chem.* **125**, 49–68 (2011).
110. Sun, J., Liu, D. Y. & Qian, S. B. A quotative research and analysis method for marine phytoplankton, An introduction to Utermöhl method and its modification. *J. Oceanogr. HuanghaianandBohai Seas* **20**, 105–112 (2002).
111. Guo, S. J. *et al.* Seasonal variation in the phytoplankton community of a continental-shelf sea, The East China Sea. *Mar. Ecol. Prog. Ser.* **516**, 103–126 (2014).
112. Welschmeyer, N. A. Fluorometric analysis of chlorophyll-*a* in the presence of chlorophyll-*b* and pheopigments. *Limnol. Oceanogr.* **39**, 1985–1992 (1994).
113. Kovach, W. L. MVSP—a multivariate statistical package for Windows, version 3.0. Kovach Computing Services, Pentraeth, Wales, UK (1998)
114. Ter-Braak, C.J.F. & Šmilauer, P. CANOCO Reference Manual and CanoDraw for Windows User's Guide, Software for Canonical Community Ordination (Version 4.5). Microcomputer Power, Wageningen. Soil macrofauna in organic and conventional coffee plantations in Brazil (2002)
115. Ortega-Retuerta, E. *et al.* Uncoupled distributions of transparent exopolymer particles (TEP) and dissolved carbohydrates in the Southern Ocean. *Mar. Chem.* **115**, 59–65 (2009).
116. Garc, C. *et al.* Hydrodynamics and the spatial distribution of plankton and TEP in the Gulf of Cdiz (SW Iberian Peninsula). *J. Plankton Res.* **24**, 817–833 (2002).
117. Bar-Zeev, E. *et al.* Transparent exopolymer particles (TEP) link phytoplankton and bacterial production in the Gulf of Aqaba. *Aquat. Microb. Ecol.* **56**, 217–225 (2009).
118. Malpezzi, M. A., Sanford, L. P. & Crump, B. C. Abundance and distribution of transparent exopolymer particles in the estuarine turbidity maximum of Chesapeake Bay. *Mar. Ecol. Prog. Ser.* **486**, 23–35 (2013).
119. Ramaiah, N. *et al.* Effect of iron enrichment on the dynamics of transparent exopolymer particles in the western subarctic Pacific. *Prog. Oceanogr.* **64**, 253–261 (2005).

Acknowledgements

This work was supported by the National Nature Science Foundation of China (41876134), the Tianjin 131 Innovation Team Program (20180314), and the Changjiang Scholar Program of Chinese Ministry of Education (T2014253) to Jun Sun. Additionally, we would like to thank the Open Cruise Project in the Western Pacific Ocean of the National Nature Science Foundation of China (NORC2017-09) for sharing their ship time. We also thank our colleagues Professor Dongliang Yuan from Institute of Oceanology of Chinese Academy of Sciences who provided insight and expertise that greatly assisted the research, although he may not agree with all of the interpretations/conclusions of this paper.

Author contributions

Full manuscript writing, figure drawing or generating, and TEP analysis was done by Dr. M.S.I. under the close supervision of professor Dr. J.S. Nutrients analysis was done by G.Z. Phytoplankton species were identified by Dr. M.S.I. and confirmed by Z.C. Manuscript design and discussion were directed by H.Z. The physical circulations of the WPO in Fig. 1 with its directions were drawn by Dr. M.S.I.

Competing interests

The authors declare no competing interests.

Additional information

Supplementary Information The online version contains supplementary material available at <https://doi.org/10.1038/s41598-021-88477-0>.

Correspondence and requests for materials should be addressed to J.S.

Reprints and permissions information is available at www.nature.com/reprints.

Publisher's note Springer Nature remains neutral with regard to jurisdictional claims in published maps and institutional affiliations.



Open Access This article is licensed under a Creative Commons Attribution 4.0 International License, which permits use, sharing, adaptation, distribution and reproduction in any medium or format, as long as you give appropriate credit to the original author(s) and the source, provide a link to the Creative Commons licence, and indicate if changes were made. The images or other third party material in this article are included in the article's Creative Commons licence, unless indicated otherwise in a credit line to the material. If material is not included in the article's Creative Commons licence and your intended use is not permitted by statutory regulation or exceeds the permitted use, you will need to obtain permission directly from the copyright holder. To view a copy of this licence, visit <http://creativecommons.org/licenses/by/4.0/>.

© The Author(s) 2021